A Simple Model for the Evaporation of Hydrometers and Their Isotopes

Simon P. de Szoeke[1], Mampi Sarkar[2,3], Estefanía Quiñones Meléndez[1], Peter N. Blossey[4], David Noone[1,5]

[1]College of Earth, Ocean, and Atmospheric Sciences, Oregon State University, Corvallis, OR, USA
[2]Institute of Climate and Atmospheric Science, University of Houston, Houston, TX, USA
[3]Department of Earth and Atmospheric Sciences, University of Houston, Houston, TX, USA
[4]University of Washington, Seattle, WA, USA
[5]Department of Physics, University of Auckland, New Zealand

Key Points:

- Evaporated vapor from rain ($\delta_D = 0$ ‰ with 0.2 of rain mass evaporated) is near the rain's initial isotope composition, strongly enriched compared to the surrounding vapor.
- Rain isotope composition quickly equilibrates to the surrounding environmental vapor.
- Small and especially vanishing drops are enriched by molecular diffusion 40% more than millimeter-sized drops.

Corresponding author: Simon de Szoeke, `simon.deszoeke@oregonstate.edu`

Abstract

Evaporation decreases the mass and increases the isotope composition of falling drops. Combining and integrating the dependence of the evaporation on the drop diameter and on the drop-environment humidity difference, the square of drop diameter is found to decrease with the square of vertical distance below cloud base. Drops smaller than 0.5 mm evaporate completely before falling 700 m in typical subtropical marine boundary layer conditions. The effect on the isotope ratio of equilibration with the environment, evaporation, and kinetic molecular diffusion is modeled by molecular and eddy diffusive fluxes after Craig and Gordon (1965), with a size-dependent parameterization of diffusion that enriches small drops more strongly, and approaches the rough aerodynamic limit for large drops. Rain shortly approaches a steady state with the subcloud vapor by exchange with a length scale of 40 m. Kinetic molecular diffusion enriches drops up to as they evaporate by up to +5 ‰ for deuterated water (HDO) and +3.5 ‰ for $H_2{}^{18}O$.

Rain evaporation enriches undiluted subcloud vapor by +12 ‰ per mm rain, explaining enrichment of vapor in evaporatively cooled downdrafts that contribute to cold pools. Microphysics enriches the vapor lost by the early and complete evaporation of smaller drops in the distribution. Vapor from hydrometeors is more enriched than it would be by Rayleigh distillation or by mixtures of liquid rain and vapor in equilibrium with rain.

Plain Language Summary

A model of evaporating rain explains enrichment of rare isotopes in water vapor observed during atmospheric cold pools below shallow convection. Rain becomes more enriched as it evaporates by exchange with subcloud vapor, by equilibrium fractionation, and by the weaker molecular diffusivity of rare-isotope water vapor. The model predicts molecular diffusion enriches the rain drops more than previously thought, especially as they near complete evaporation.

1 Introduction

Clouds transport water from the subcloud boundary layer and condense and detrain it in and above the planetary boundary layer. Models for hydrometeor (cloud and rain drop) evaporation are useful for characterizing vapor sources and inferring cloud and rain processes. Condensation and evaporation processes fractionate the ratio of total water molecules to its rare isotopologues. ($H_2^{18}O$ contains the oxygen-18 [^{18}O] isotope and deuterated water HDO contain the deuterium [D or ^2H] isotope.) Combinations of sources and processes yield particular water vapor and precipitation isotope ratios (e.g., Dansgaard, 1964; Gat, 1996; Noone et al., 2012; Tremoy et al. 2014; Crawford et al. 2017), yet the problem of inferring the history of water from observed or modeled isotopes is confounded by complex and ambiguous combinations of sources and processes (Galewsky et al., 2016; Hiron and Flossman, 2020).

This complexity is reduced for idealized cases, such as mixing, Rayleigh distillation of water vapor by condensation, precipitation, and the predictable combination of vapor exchange, equilibrium fractionation, and diffusion accompanying evaporation (Craig and Gordon, 1965; Stewart, 1975). The equations predicting isotopic fractionation during rain evaporation in weather and climate models (Noone et al., 2012; Blossey et al., 2010; Risi et al., 2021; Sengupta et al., 2023) are numerically integrated to simulate observed cases and process studies (e.g., Salamalikis et al., 2016; Graf et al., 2017; Sarkar et al., 2023). The isotope ratio depends strongly on the fraction of the drop that evaporates, allowing the isotope evaluation to be conveniently separated from evolution of the drop mass (e.g., Hiron and Flossman, 2020).

Here we model the evaporation of hydrometeors (rain drops and cloud droplets) to interpret isotope observations in precipitation and water vapor observed in atmospheric cold pools (Quiñones Meléndez et al., 2024). The observations are summarized in section 2. A model for evaporation of atmospheric hydrometeors is presented that solves for isotope concentration of rain drops and of evaporated vapor from the drops, in section 3. Section 4 presents results of the model. The solutions show two regimes: In the *falling* regime a small fraction of the drop evaporates as it falls through the environment. In the *vanishing* regime the remaining hydrometeor completely evaporates as its fall speed goes to zero. A simulation is used to interpret rain and downdraft vapor observed during the EUREC4A-ATOMIC (Elucidating the role of clouds–circulation coupling in climate - Atlantic Tradewind Ocean Mesoscale Interaction Campaign) field experiment (Stevens et al., 2021). Sensitivity experiments to initial conditions and microphysics demonstrate and isolate distinct effects on the isotopes by exchange with surroundings, equilibrium fractionation, and differential diffusion. Section 5 summarizes the article.

2 Observations of a cold pool

Compared to the varied processes that contribute to the isotope ratio of precipitation and water vapor in the atmosphere, a relatively simple set of processes contributes to warm (nonfreezing) marine trade cumulus clouds, allowing us to isolate the effect of local water vapor sources. We simulate the hydrometeor evaporation leading to an atmospheric cold pool observed under shallow winter tropical trade cumulus clouds over the western Atlantic Ocean during EUREC4A-ATOMIC (Quinn et al., 2021; Bailey et al., 2023; Quiñones Meléndez et al., 2024). Figure 1 shows the time series at 1-minute resolution of a cold pool observed on Feb 10, 2020 around 16:00 UTC aboard the NOAA research vessel *Ronald H. Brown*. With air temperature cooling by 2.5 °C, this cold pool is among the strongest events observed on the ship while isotope measurements were available. Rain fell at the ship during the temperature front and minimum, suggesting the cold air and slight moistening of the specific humidity (Fig. 1b) were caused by the evaporation of hydrometeors. Water vapor isotope ratios (δ D and ^{18}O, Fig. 1c,d) are enriched in the cold pool compared to the background subcloud vapor measured before the cold pool. Three rain samples were promptly collected in rain showers at 16:15, 16:25, and 16:40 UTC, and later analyzed to have δ_D = 15.5, 14.5, and 16.2 ‰and $\delta_{18}{}_O$ = 0.17, 0.87, and 0.4 ‰ (blue dots show the equivalent equilibrium vapor $\delta_{eq.v} = \alpha_e(\delta_L+1)-1$ in Fig. 1c,d), with $alpha_e$ computed at T = 295 K. This is one of the strongest cold pools among those for which Quiñones Meléndez et al. (2024) analyzed the sources of potential temperature, specific humidity, and isotope ratio. Having synchronous and collocated observations of rain, cold temperature, and enriched isotope ratios, the Feb 10, 16 UTC event excels for studying water vapor from freshly evaporated hydrometeors.

We construct a case for evaporation of hydrometeors below cloud, adopting initial conditions from Sarkar et al. (2023; called Sarkar23; Table 1). Drops are released from cloud base at 700 m and fall through a layer of uniform specific humidity with q_v 12.9 g kg^{-1}. Because the temperature increases adiabatically downward, environmental relative humidity is saturated at cloud base and 0.69 at the surface. The isotope ratio of the initial drop liquid $\delta_{D,L0} = 8.68$ ‰ is taken to be in equilibrium with vapor ($\delta_{D,v0} = -73$ ‰) measured on the WP-3 aircraft (Sarkar et al., 2023).

We modify the subcloud layer water vapor in case CP slightly from Sarkar23 to match the background surface vapor of $\delta_{D,17\mathrm{m}} = -69.7$ ‰ observed before the cold pool (Fig. 1). Humidity and isotopes are taken to be mixed by subcloud layer-scale eddies above the surface layer. The height of the isotope analyzer inlet (18 m) is within the surface layer, so it will be more enriched than most of the subcloud layer due to gradients near the ocean (e.g., Thurnherr et al. 2020). We adjust humidity and isotopes by integrating the gradients through the constant-flux surface layer (Garratt, 1992), and average the result for

Figure 1. Ship time series containing a cold pool from 2020 Feb 10 15:40-17:00 UTC. (a) air temperature (°C), rain rate (cyan shaded, mm h^{-1}), and (b) specific humidity (g kg^{-1}) at 17 m. (c) δ deuterium (‰ = 10^{-3}) and (d) δ oxygen-18 sampled at 18 m. Rain liquid was collected promptly during rain showers at 16:15, 16:25, and 16:40; and subsequently analyzed. Vapor isotope ratio $\delta_v = \alpha_e(\delta_L + 1) - 1$ in equilibrium with the rain is shown by blue dots in (c) and (d).

Table 1. Initial conditions at cloud base (saturated) and subcloud vapor conditions for case Sarkar23 (Sarkar et al., 2023) and case CP (2020 Feb 10, 16 UTC). Subcloud air is adiabatically stratified and uniformly has the specific humidity and isotope ratio of the surface. Vapor in cloud and subcloud air are observed by aircraft for Sarkar23; the corresponding equilibrium liquid is computed. CP uses initial rain liquid from Sarkar23. CP observations of vapor from the isotope analyzer before the cold pool are adjusted to the subcloud mean with flux-gradient similarity theory; equilibrium liquid is computed. CP rain is observed and the corresponding equilibrium vapor is computed.

	z (m)	T (K)	q_v (g kg^{-1})	$\delta_{\mathrm{D,liq}}$ (‰)	$\delta_{\mathrm{D,vap}}$	$\delta_{\mathrm{18O,liq}}$	$\delta_{\mathrm{18O,vap}}$
case Sarkar23							
cloud base vapor	700	290	12.9	8.68	-73	-1.75	-11.7
subcloud vapor	0	296.8	12.9	4.54	-70	-1.14	-10.5
rain liquid modeled	0	296.8	-	15.8	-59.6	2.03	-7.36
case CP							
cloud base vapor	700	290	12.9	8.7	-73	-1.75	-11.7
subcloud vapor	0	296.8	12.9	4.1	-70.3	-1.02	-10.4
rain liquid modeled	0	296.8	-	15.4	-60.2	2.14	-7.24
rain liquid observed	0	296.8	-	15.4	-60.0	0.7	-8.7

150-700 m. This gives a subcloud deuterium isotope ratio of $\delta_{D,\mathrm{subcloud}} = -70.3$ ‰, very close to Sarkar23's $\delta_{D,\mathrm{subcloud}} = -70$ ‰ (Table 1).

3 Model

Following Best (1952; and, e.g., Abraham, 1962; Li and Srivastava, 2001), the prognostic drop evaporation model evaluates the change of the square of the drop diameter as a function of the temperature and humidity of the environment. The model parameterizes diffusive kinetic effects that depend on empirical drop ventilation factors, the hydrometeor fall speed (Graf et al., 2017), and a vertically varying environment. We obtain analytical functions accurate within a neighborhood of drop diameter and height below cloud. Isotope ratios are calculated from the drop diameters with the Craig and Gordon (1965) model.

3.1 Drop diameter and mass

Sarkar et al. (2023) integrates prognostic equations for the mass, temperature, and isotope ratios of liquid water drops evaporating as they fall from cloud base to the surface for several drop size distributions and environmental profiles observed from the NOAA WP-3 aircraft in EUREC4A-ATOMIC (Pincus et al., 2022; Bailey et al., 2023). We simulate the 2020 Feb 9 case, approximating the drop size distribution (DSD) by the log-normal distribution of Sarkar et al. (2023; section 3.4).

The Lagrangian prognostic equations for the drop are transformed from time derivatives to vertical derivatives by dividing by the fall speed $U_{\mathrm{fall}} = -dz/dt > 0$. The equation for drop diameter D evaporating into surrounding air with temperature T_a and vapor density $\hat{\rho}_{va}$ is (Salamalikis et al., 2016; Graf et al., 2017),

$$\frac{dD}{dz} = \frac{4 f_v K_{va}}{D U_{\mathrm{fall}} \hat{\rho}_l R_v} \left(\frac{e_s(T_r)}{T_r} - \mathrm{RH} \frac{e_s(T_a)}{T_a} \right) = \frac{4 f_v K_{va}}{D U_{\mathrm{fall}} \hat{\rho}_l} (\Delta \hat{\rho}_v), \tag{1}$$

where f_v is the ventilation factor (Stewart, 1975), K_{va} the kinematic diffusivity of vapor in air, and T_r is the drop surface temperature and $e_s(T)$ is the saturation vapor pressure, RH is relative humidity, and $\Delta\hat{\rho}_v = \hat{\rho}_{vr} - \hat{\rho}_{va} > 0$ is the vapor density difference between the air and the drop surface. In this equation, $dD/dz > 0$ because the drops shrink as they fall.

We write equation (1) in terms of the uniform specific humidity, assuming a well-mixed subcloud layer and adiabatic temperature below cloud. The drop temperature approaches the wet bulb temperature (Appendix B). Linearizing the saturation specific humidity and the wet-bulb temperature lapse rate Γ_w yields

$$\frac{dD}{dz} = \frac{4 f_v K_{va}}{D U_{\text{fall}} \hat{\rho}_l} \left(\frac{\partial q_s}{\partial T} \right)_{\tilde{T}} \Gamma_w z'.$$

Then, the drop evaporation equation is divided into one factor that depends on D on the left hand side, and another that depends on the vertical displacement from cloud base on the right hand side:

$$-a(D) D \, dD = z' \, dz', \tag{2}$$

with

$$a(D) = \frac{\hat{\rho}_l}{4 K_{va} \Gamma_w (\partial q_s / \partial T)_{\tilde{T}}} \frac{U_{\text{fall}}}{f_v}. \tag{3}$$

The factor a is nearly a constant, as the quotient U_{fall}/f_v is a slowly varying function of diameter. For drops larger than 0.5 mm $U_{\text{fall}}/f_v \approx 0.9$ m s^{-1}. At smaller diameter, the fall velocity vanishes faster than the ventilation factor, and $a(D)$ (equation 3) becomes very small.

Solutions of equation (2) describe elliptical arcs centered at $D = 0, z' = 0$ (Fig. 2).

$$-a(D^2 - D_0^2) = z'^2 - z'^2_0 \tag{4}$$

Best (1952) encapsulates the effect of the environment, mainly the saturation deficit, in a local "evaporation radius" K on the right hand side, $D_1^2 - D_2^2 = 4K^2$. The drop diameter-displacement curves are elliptical because saturation deficit increases linearly with distance from cloud base $4K^2 = a^{-1}(z_2'^2 - z_1'^2)$. Small departures from the linear dependence on height such as fall speed and ventilation are contained in a. Numerical solutions of 4 show the curves of radius vs. height are nearly ellipses (Fig. 2b and Fig. 1 of Abraham et al., 1972), but flatten out as drops vanish and their fall speed goes to zero.

Drop vanishing. The function $a(D)$ varies little for $D > 0.4$ mm. But in the Stokes (1851) viscous drag regime, when drops get smaller (Re<5), the fall speed $U_{\text{fall}} \propto D^2$ and $a(D)$ vanish over small vertical displacements. This squashing of the displacement near vanishing due to the dependence on U_{fall}/f_v, can be parameterized by the function

$$a \approx a_0 \frac{D^2}{D^2 + b^2}, \tag{5}$$

with $a_0 = 2.1 \times 10^{12}$ and $b = 0.2$ mm. This approximation estimates the displacement at which drops vanish. The vanishing factor $D_1^2/(D_1^2 + b^2)$ approaches unity in the falling regime.

The quasi-elliptical trajectories of drop diameter vs. displacement fallen can be evaluated in midpoint prediction-correction steps of drop diameter. It is accurate to evaluate in a few ($k_{\max} = 5$) cosine-spaced steps $D_k = D_0 \cos(\pi k/(2k_{\max}))$ (Fig. 2b, circles). However, to find the resulting size of all drops at each height, we use 1 m vertical resolution (Fig. 2b, lines). The 5-step evaluation agrees with the high-resolution solution because the slope $a(D)$ varies slowly. A single step ($k_{\max} = 1$) overestimates the displacement that small drops fall because of the curvature of $a(D)$ for $D \lesssim b \approx 0.2$ mm. The approximation for a (equation 5) accurately predicts the displacements at which drops completely evaporate.

Figure 2. (a) The lognormal drop number $N(D)$ and mass size distributions. (b) Traces of individual diameters D from initial cloud-base ($z = 700$ m) diameters D_0 by numerical stepping of the quadratic equation. (c) Mass fraction remaining as a function of height and initial diameter. The dashed line shows $D = 0.14$ mm where Re ≈ 5, for which drops with smaller diameters rapidly vanish in small displacements.

3.2 Isotope exchange

The change in the isotope ratio of a single liquid drop is calculated from the mass fraction $f = (D/D_0)^3$ of drop liquid remaining, using the Craig and Gordon (1965; and Stewart, 1975) model. Single-drop results are then integrated over the drop size distribution.

Craig and Gordon (1965) and Stewart (1975) assume finite diffusion between the equilibrium vapor over the drop and the surrounding air. The drop isotope ratio R_L is predicted by

$$R_L - cR_{air} = (R_{L0} - cR_{air})f^A, \tag{6}$$

where f is the mass fraction of the drop remaining. The exponent is

$$A = \frac{\rho}{\rho_i}\frac{\alpha_e}{1-h} - 1.$$

where $\alpha_e = R_V/R_L < 1$ is the (equilibrium) fractionation factor of vapor over liquid. The coefficient c is

$$c = \frac{h}{\alpha_e - (1-h)(\rho_i/\rho)}. \tag{7}$$

Including exchange with environmental vapor and diffusive effects replaces α_e in the Rayleigh process with $\alpha_e(\rho/\rho_i)/(1-h)$. Rayleigh evaporation assumes vapor at equilibrium over the drop irreversibly leaves the drop as it evaporates. The isotope ratio of the liquid is then fractionated (Rayleigh):

$$R_L = R_{L0}f^{\alpha_e - 1}.$$

The initial condition for equation 6 is $f = 1$. As $f \to 0$,

$$R_{L\mathrm{end}} = cR_{air}. \tag{8}$$

For saturation fraction $h = 0$, cR_{air} drops out, giving $R_L = R_{L0}f^{\alpha_e\rho/\rho_i - 1}$. which is like the Rayleigh solution, except for ρ/ρ_i in the exponent.

3.3 Kinetic effect of diffusion from evaporating drops

A spherical drop evaporates by a sum of diffusion by molecular diffusivity K_m and eddy diffusivity K_e. The molecular diffusivity varies for different isotopes, the eddy diffusivity K_e depends on the flow around the drop, but is the same for all species. Moreover, the ratio of resistances $\rho_i/\rho = 1 + n(K_m/K_{mi} - 1)$ of flux of the rare isotopologue to the flux of abundant water vapor depends on the drop size through the ratio of molecular to total (molecular + eddy) resistance $n = \rho_m/\rho$. The diffusivity ratio K_{mi}/K_m from Merlivat (1978) is 0.9755 for deuterium and 0.9723 for oxygen-18. Stewart (1975) and Kinzer and Gunn (1951) found $n = 0.58$ for drops in the range 1.4-2.8 mm diameter.

For spherical symmetry and steady conditions, the drop evaporation flux E is a product of the diffusivity K and the radial derivative of saturation fraction $h = \hat{\rho}_v/\hat{\rho}_{\mathrm{vsat}}$,

$$E = -\frac{1}{\hat{\rho}_{\mathrm{vsat}}}\frac{dm}{dt} = -4\pi r^2 K\frac{dh}{dr},$$

where $\hat{\rho}_v$ is vapor density. Integrating the humidity h from the drop surface radius a where $h = 1$ gives the humidity $h(r)$ as a function of distance from the drop,

$$1 - h(r) = \int_r^a dh = \frac{E}{4\pi}\int_r^a \frac{1}{K}\frac{dr'}{r'^2} = \frac{E}{4\pi}\frac{1}{K}\left(\frac{1}{a} - \frac{1}{r}\right). \tag{9}$$

We model the diffusion through spherical shells, with molecular diffusivity K_m from the drop radius a through a laminar layer of thickness l, and with eddy diffusivity K_e outside radius $a + l$. The area-integrated nondimensional vapor flux through the shell is, uniform with radius, $E = (1 - h)/\rho$. It depends only on the saturation deficit and resistance $\rho = 1/(4\pi K a)$.

Integrating at shells of different radii gives $\rho = \rho_m + \rho_e$ with

$$\rho_m = \frac{1}{4\pi K_m a} \frac{l}{a + l} \quad \text{for} \quad r = [a, a + l],$$

and

$$\rho_e = \frac{1}{4\pi K_e} \frac{1}{a + l} \quad \text{for} \quad r = [a + l, \infty).$$

This spherical model of diffusion yields the ratio of molecular to total resistance,

$$n = \frac{\rho_m}{\rho} = \left(1 + \frac{K_m}{K_e} \frac{a}{l}\right)^{-1},$$

that depends on the ratio a/l of the drop size to a viscous-diffusive length scale l. Vapor diffuses away from small drops through concentric shells, as above, in a laminar layer of thickness $l_\nu = \nu/U$. The velocity U balances drag with gravity and turbulent inertial accelerations.

Diffusion through this spherical geometry predicts vanishingly small drops approach $n = 1$. Flow separates from large drops and the diffusion loses its spherical geometery. Choosing total thickness

$$l = l_\nu + l_e,$$

with $l_e = (K_m/K_e)a$, matches the rough limit $n = 1/2$ for large drops (Brutsaert, 1965; 1975; Merlivat and Jouzel, 1979). Molecular to eddy vapor diffusivity ratio $K_m/K_e = 6 \times 10^{-3}$ matches the experimental results, for drops of diameter 1.4, 2.1, and 3 mm, of Kinzer and Gunn (1951) and Stewart (1975) (Fig. 3 solid). We use this first parameterization. An ad hoc alternative parameterization matching the experiments, that asymptotes instead to $n = 0.55$ for large drops, is $\tilde{n} = 0.55 + 0.45(1 + 0.04a/l_\nu)^{-1}$ (Fig. 3 dashed).

Models such as Lee and Fung (2008), Graf et al. (2019), and Sarkar et al. (2023) include the effect of differential diffusion through empirical ventilation factors that depend on the diffusivity of each isotopologue species. Our approach follows Stewart (1975), resolving kinetic effects by explicitly parameterizing the flow- and geometry-dependence of the ratio of laminar and turbulent resistances. Where Stewart had determined this experimentally for 1-3 mm drops, we parameterize the effect as a function of the size of any falling drop. This explicit treatment of diffusivity predicts kinetic effects on the isotopes of drops even as they vanish.

3.4 Drop size distribution

We evaluate the diameter of drops sampled from a drop size distribution (DSD). The initial DSD is the lognormal distribution

$$N(D_0) = N_0/(D_0\sqrt{2\pi\sigma^2}) \exp(-(\log(D_0) - \mu)^2/(2\sigma^2)), \tag{10}$$

observed from aircraft in Atlantic trade wind shallow cumulus clouds in EUREC4A-ATOMIC. The drop number concentration $N_0 = 500$ m^{-3}, the lognormal width is $\sigma = 0.35$, and the lognormal mode $\mu = \log(D_g)$ is the log of the geometric mean diameter $D_g = 0.22$ mm, equivalent to the DSD of Sarkar et al. (2023), but with alternate notation. Figure 2a shows this DSD. Substitution of D from equation 4 could be used to derive the evolution $N(D)$ of the DSD with time. However, since resolving the vanishing behavior of drops

Figure 3. Resistance ratio $n = \rho_m/\rho$ parameterization (solid), ad hoc empirical parameterization n_{emp} (dashed), with lab experiment results of Kinzer and Gunn (1951; circles) and Stewart (1975; circle and whisker).

Figure 4. (a) Mass fraction of total liquid remaining vs. height. (b) Mean deuterium δ (‰) of all the liquid remaining. (c) Deuterium δ of drop evaporation at each height (dot-dashed) and cumulative evaporated vapor (solid). Black dashed (c) shows the isotope ratio of the surrounding vapor.

is important, we explicitly simulate predict the diameter change of 161 drops, initially geometrically spaced with diameters D_0 between 11×10^{-6} m and 33 mm. This set of drops resolves the tails of the DSD. Drop diameters D are evaporated by equation 4. Drops initially smaller than $D_{0\mathrm{crit}} = 0.51$ mm evaporate completely within 700 m below cloud base.

4 Isotope results

We evaluate the isotope ratio R_L of each drop using the mass fraction f and equation 6 for the cold pool case (CP, Table 1). The total mass fraction, and deuterium composition of the remaining DSD and the vapor lost is shown in Fig. 4. Figure 4c shows the deuterium composition of the immediately evaporated vapor (dot-dashed) and the cumulative vapor (solid), compared to the surrounding subcloud vapor (black dashed) in delta notation $\delta = R/R_{\mathrm{standard}} - 1$. The cumulative vapor below 650 m is enriched compared to the surroundings. It is enriched to $\delta = 0$ ‰ below 500 m. A small fraction of this enriched vapor could explain the enrichment observed in cold pools in Fig. 1. The immediately evaporated vapor at each level is yet more enriched.

The isotope ratio is shown for 10 drops with diameters of 0.13 to 4.8 mm (Fig. 5). The initial isotope ratio is $\delta_{\mathrm{DL0}} = 8.68$‰, $\delta_{^{18}\mathrm{OL0}} = -1.75$‰ (‰ $\equiv 10^{-3}$). Drops enrich monotonically as they fall and evaporate fractionally more of the lighter H_2O isotopologues. Curves that strike $z = 0$ reach the surface. The largest drop shown (4.8 mm; cyan left) nearly reaches $\delta_{\mathrm{D}} = 10$‰ at the surface. Smaller drops fall slower, evaporate fractionally more and become more enriched over a shorter distance. The smallest drop shown (blue, top) quickly reaches equilibrium with the surrounding vapor, before evaporating completely between 500-600 m. The largest drop shown here that evaporates completely (0.44 mm, red) enriches to $\delta_{\mathrm{D}} = 16$ ‰, where it vanishes around 150 m. The enrichment curves for water containing deuterium or oxygen-18 isotopes appear quite similar, differing mostly due to the difference between isotope ratio of the initial drop and the equilibrium liquid isotope ratio of the air (at the intersection of the black lines at cloud base), which is stronger, relative to its kinetic effect, for deuterium than for oxygen-18.

All drops enrich by exchange with the surrounding vapor, from the drop initial condition, toward equilibrium with the vapor. The equilibrium liquid isotope ratio of the air at $h = 1$ (shown at z=700 m) is $\delta_{\mathrm{D,end}} = 11.6$‰, $\delta_{^{18}\mathrm{O,end}} = -0.42$‰ for subcloud air vapor isotope ratios $\delta_{\mathrm{D,air}} = -70.3$‰, $\delta_{^{18}\mathrm{O,air}} = -10.4$‰. Large drops fall through the layer exchanging only slightly, while small drops exchange quickly toward equilibrium with the enriched ambient vapor. Lee and Fung (2008) use the rate at which drops reach isotopic equilibrium with relatively enriched environmental vapor as a possible explanation for the amount effect phenomenon, where precipitation is relatively depleted at higher precipitation rates (Dansgaard, 1964).

In addition to exchange and equilibration, kinetic effects (Fig. 5) result in small drops reaching a yet more enriched end point at lower relative humidity, where the "end point" is the asymptotic value of the raindrop isotopic composition as $D \to 0$. The heavier water isotopologues diffuse away from the drops more slowly than $H_2^{16}O$, enriching

them. The black lines show the end point isotope ratio of liquid drops predicted by different parameterizations of the kinetic fractionation (i.e. different values of n). At cloud base (700 m, $h = 1$) all endpoint curves intersect the vertex of equilibrium with the environmental vapor. Drops approach their end point isotope ratio $R_{\rm end} = cR_{\rm air}$ (thin black line) predicted by equation 7. The kinetic effect of differential diffusion is stronger as n approaches unity, for small drops. The isotope ratio $R_{\rm air}h/[\alpha_e - (1-h)]$ (black dot-dashed) is the end point for the artifical case of $n = 0$, which would be obtained were the isotope diffusivity equal the ordinary vapor diffusivity.

Estimates of $R_{\rm end}$, using our n parameterization to model ρ_i/ρ, for large (4.8 mm) drops (black solid), agree with results for $n = 0.58$ (black dashed), found for lab experiments on drops larger than 1 mm diameter (Stewart, 1975). The $n = 0.58$ end point underestimates kinetic enrichment as drops shrink. Even drops as small as 0.13 mm fall more than 100 m with their isotope ratio greater than the endpoint $R_{\rm end}$ predicted by $n = 0.58$. The enrichment of $\delta_{\rm end}$ is approximately proportional to n. Our parameterization for n, which approaches $n = 1$ and $(\rho_i/\rho = K_m/K_{mi})$ for small drops has about 42% more kinetic enrichment than taking constant $n = 0.58$.

Though the mass of vanishing drops is small, rain transports enriched liquid downward, leaving relatively depleted vapor near cloud base. Small drops and virga experience the strongest enrichment and their complete evaporation moves very enriched vapor downward in the subcloud layer. Virga that evaporates just before reaching the surface is enriched, by +7 ‰ for deuterium and by +5 ‰ for oxygen-18, with kinetic effects of +5.8 ‰ and +3.5 ‰, respectively. This evaporation of enriched hydrometeors (both large and small) explains enrichment of vapor observed in evaporatively cooled cold pools in EUREC4A-ATOMIC (section 2).

Equilibration and kinetic effects reduce deuterium excess (DXS, Fig. 6) of drops as they fall, because the loss to evaporation of HDO is more efficient than the loss of $H_2{}^{18}O$, enriching the drops relatively more in $H_2{}^{18}O$ than predicted by the global meteoric water line. DXS of the equilibrium ($n = 0$) end point is 8 ‰ lower in the subcloud vapor than in the initial drop condition, but the DXS is reduced by 20 ‰ by drops that undergo significant kinetic enrichment.

The rain evaporation process, replete with kinetic evaporation, does not describe a meteoric water line with nearly constant DXS $= \delta_{\rm D} - 8\delta_{\rm 18O}$. Figure 7 shows isotope δ trajectories of evaporating drops have continuously decreasing DXS. The first adjustment from initial liquid ($\delta_{\rm D} = 8.7$ ‰) toward 11.6 ‰ is due to exchange with the surrounding vapor, so its slope depends strongly on those prescribed conditions, rather than on any physical process. In the kinetic enrichment limit for small drops ($n \to 1$), $\delta_{\rm D}$ increases in proportion to $1.4\delta_{\rm 18O}$. As drops vanish, they approach a nearly constant $y = \delta_{\rm D} - 1.4\,\delta_{\rm 18O}$ of the surrounding vapor, of about $y_{\rm end} = 12.1$ ‰. The limits $\delta_{\rm end} = cR_{\rm air}/R_{\rm std} - 1$ for deuterium and oxygen-18 of small drops and constant subcloud vapor $R_{\rm air}$ shows the linearity of $\delta_{\rm D}$ and $\delta_{\rm 18O}$ (Figure 5) depends on the ratio of $c_{\rm D}/c_{\rm 18O}$. Changes in saturation h over the drop and $\alpha_e(T)$ with height are responsible for the compensated changes of $\delta_{\rm D}$ and $1.4\delta_{\rm 18O}$ along $y_{\rm end}$.

4.1 Vapor lost by hydrometeors

The instantaneous and cumulative isotope ratio of the vapor evaporated from all hydrometeors in the DSD is shown as a function of height in Fig. 4b and c, and as a function of the mass fraction of original hydrometeor liquid in 8. Experiments show the isotope ratio of the vapor lost by the drops is dominated by equilibrium and kinetic fractionation, and secondarily by the DSD. The Craig and Gordon evaporation equation (CG; equation 6) generates concave-down curves that enrich quickly at first, i.e., at low mass fraction evaporated, and then slowly approach the isotope ratio of the original liquid δ_{D0}. The CG model for a single drop, or equivalently a monodisperse DSD (brown), is still

Figure 5. (a) Deuterium and (b) oxygen-18 isotope trajectories (colored lines) for drop with initial diameter D_0 of 0.13 (blue, top), 0.20, 0.29, 0.44, 0.65, 0.97, 1.45, 2.2, 3.2, and 4.8 (cyan, lowest) mm. Our parameterization for the end point $R_{\rm end} = cR_{\rm air}$ for vanishing drops with $n \to 1$ (thin black). No kinetic effect $\rho_i/\rho = 1,\ n = 0$, equilibrium fractionation only (dot-dashed black). $R_{\rm end}$ for $n = 0.5$ (thin dotted black) and $n = 0.58$ (Stewart, 1975; dotted black), which matches extrapolating our model for diffusion of large (4.8 mm) drops (black solid).

Figure 6. Deuterium excess DXS = $\delta_D - 8\delta_{^{18}O}$ profiles as in Fig. 5.

Figure 7. Isotopic trajectory of the kinetic evaporation process. The vertical axis is $y = \delta_{\mathrm{D}} - 1.4\,\delta_{18\mathrm{O}}$. Black lines represent constant DXS (thick solid), and the steady state end points as in Figs. 5-6. Vanishing drops tend toward a nearly constant y.

concave-down. The shape of these curves is mostly due to the CG physics, not the shape of the DSD.

4.1.1 Sensitivity to the DSD

The standard (D_g=0.22, σ=0.345) drop size distribution is shown in blue. Results are not sensitive to narrowing the DSD's lognormal width σ by a decade, or doubling the geometric diameter D_g. The orange curve shows a narrower distribution, with width σ=0.0345 decimated. A wider σ=3.45 distribution barely evaporates, and almost all liquid remains at the surface (green; almost invisibe at left), because much of the mass is in drops too large to evaporate. The effect of the width on the isotopes is not monotonic: The narrower and wider distributions both evaporate less and enrich faster than the standard DSD.

Doubling D_g to 0.44 mm (red) reduces fraction of rain evaporated b etween cloud base and the surface to $f \simeq 0.55$. Vapor also enriches slightly more slowly, suggesting relatively more evaporation from larger less enriched drops than from the control DSD.

A case with a single drop, equivalent to a monodisperse DSD, shows the vapor resulting from the initial drop size (D_0=0.51 mm) that completely evaporates at the surface. Preferential and near-complete evaporation of the smaller drops of the DSD are responsible for about +10 ‰ more enrichment of the cases with a DSD, compared to the case with a single drop.

4.1.2 Sensitivity to the environmental profile

The case indicated by the dashed purple line uses uniform $h = 0.95$ (representative of 400 m), to simplify the effect of the environment. The main difference is that it starts off evaporating near isotopic equilibrium, compared to the transient strongly depleted vapor right below cloud base where h is nearly unity (blue line, off scale). Away from cloud base, the uniform environment has only a small effect on the isotope ratio of the evaporated vapor.

4.1.3 Comparison to simpler models

The simplest model for the isotope ratio of vapor is linear mixing between the initial liquid and its equilibrium vapor. Mixtures between the "first whiff" of initial equilibrium vapor, and the "final gulp" of completely evaporated drops appear between the straight black lines. The equilibrium varies slightly with h: the lower (solid) mixing line represents equilibrium at cloud base $h = 1$, and the upper dashed line represents the equilibrium at the surface $h = 0.89$.

The Rayleigh model for a single drop is concave up (purple dotted). This single-drop Rayleigh model performs worse than linear mixing (black lines). Rayleigh evaporation for drops in the EUREC4A-ATOMIC DSD (blue dotted) is concave down. Accounting for the DSD, the Rayleigh model is significantly improved, falling between between linear mixing and the more physical CG solutions. The vapor equilibration and kinetic fractionation effects additionally included in the CG model have a stronger effect on the results than the DSD. Evaluating CG even for a single average-sized drop gives a considerably better result than the Rayleigh model.

4.2 The rain isotope flux and source

Figures 4 and 8 show the integrated effect of rain is to enrich rainwater quickly below cloud (because the initial rain isotopic composition was in equilibrium with somewhat more depleted cloud layer air), and then evaporate this enriched water lower in the

Figure 8. Total isotope δ of vapor evaporated from rain drops, as a function of fraction f of rain mass remaining, modeling microphysical evaporation of drop mass, Craig and Gordon isotope evaporation model, with diameter-dependent kinetic effect (blue). Sensitivity studies have DSD with 10× narrower (orange) or wider (green) lognormal width σ, 2× larger geometric mean diameter D_g, surroundings with fixed T and $h = 0.95$ representative of 400 m (purple dashed), and for the single drop of initial diameter of 0.51 mm (brown). Mixtures of $f = f_{\mathrm{eq}}$ equilibrium vapor from negligibly evaporated drops and $1 - f = f_{\mathrm{complete}}$ vapor from completely evaporated drops of initial liquid isotope ratio (black: solid for vapor equilibrium over the drop evaluated at cloud base [700 m] and dashed for vapor equilibrium evaluated at the surface). Rayleigh evaporation of the control case DSD (blue dashed), and a monodisperse DSD (single drop, brown dashed).

subcloud layer. This suggests a downward flux of heavy isotopes by the rain. This upgradient flux acts to strengthen the observed depletion of heavy isotopes with altitude in the atmosphere.

The vertical flux of water isotopes by the rain is quantified from the model simulations:

$$F_{\delta\text{rain}} = \sum_j M_j(\delta_j - \overline{\delta}), \tag{11}$$

where $M_j = -(\pi/6)\hat{\rho}_l D_j^3 U_{\text{fall},j} N_j$ is the mass flux of drops of diameter D_j with the drop number concentration of per unit volume of air, $N_j = N(D_{0,j})$, given by the initial DSD.

In our steady state model, the total water isotope source, to the air-rain mixture due to the rain, is the convergence of the rain isotope flux,

$$S_{\delta\text{rain}} = -\frac{1}{\hat{\rho}_v}\frac{\partial}{\partial z}F_{\delta\text{rain}} = \frac{1}{\hat{\rho}_v}\sum_j\left[-\frac{\partial M_j}{\partial z}(\delta_j - \overline{\delta}) - M_j\frac{\partial}{\partial z}(\delta_j - \overline{\delta})\right], \tag{12}$$

where $\hat{\rho}_v$ is the vapor density per unit of total air and $\overline{\delta}$ is the mean isotope δ of total water, which is dominated by the subcloud vapor. The source is separated into two physically distinct parts: on the left, the effect of bulk rain evaporation, and on the right, the effect of advection of the isotopes by the rain.

The mass flux, isotope flux, and source rates all scale with the rain rate (and N_0); the integrated source scales with the rain accumulation. We evaluate the rain flux of δ for the deuterium isotope for a nominal rain rate of $M_j/\hat{\rho}_l = 1$ mm h^{-1} (Fig. 9a), and the integrated source for 1 mm of precipitation accumulation at the surface (Fig. 9b)

The weaker term of the flux divergence is the advection of the isotope by the rain. Since the mean $\overline{\delta}$ is nearly constant, the effect of the advection term is mostly within the liquid phase. Drops enrich by evaporation and exchange, especially near cloud base, causing strongly negative $\partial\delta_j/\partial z$. This gradient results in negative isotope advection by the falling rain.

The stronger term is the evaporation (Fig. 9b, red). Removing rain mass causes convergence of the rain mass flux. Drops are enriched compared to the subcloud vapor, explaining the large enrichment by the evaporation. The vertically averaged subcloud rain evaporation source enriches an undiluted precipitating core by +11.8 ‰ per mm rain. The precipitation accumulation for the cold pool on Feb 10, 16 UTC (Fig. 1a) is 1.9 mm. Evaporation from this accumulation would enrich precipitation downdraft core by air by 22 ‰. This contributes to the cold pool, whose deuterium δ is enriched by +4.9 ‰ (Fig. 1c). Were the hydrometeor evaporation the only source, dilution of the evaporative core by 3.6 times as much surrounding air would explain the vapor isotopes observed in the cold pool. In fact, other sources in addition to hydrometeor evaporation, such as evaporation from the ocean surface, also contribute to the near surface air in cold pools (Quiñones Meléndez et al. 2024).

4.3 Sensitivity to isotope ratio of the initial drop and subcloud vapor

The rain at the surface is largely equilibrated through exchange with the vapor in the subcloud air. This exchange was identified in early isotope-enabled general circulation models as a factor for predicting local precipitation-temperature relationships (e.g., Noone and Simmonds, 2002). Experiments varying the initial drop isotope ratio, and varying the isotope ratio of the vapor in the subcloud air show the isotope ratio of the surface rain (integrated over the DSD) depends strongly on the isotope ratio of the vapor in the air, and slightly on the drop initial conditions. The sensitivity for deuterium anomalies is

$$\delta'_{\text{pcp,sfc}} = 0.972\alpha_e^{-1}\delta'_{\text{air}} + 0.036\delta'_{L0}, \tag{13}$$

with $\delta' = \delta - \delta^\circ$ indicating anomalies from reference conditions δ°, which are for the standard cold pool case: $\delta^\circ_{\rm pcp,sfc} = 15.4$ ‰, $\delta^\circ_{\rm air} = -70.3$ ‰, and $\delta^\circ_{L0} = 8.68$ ‰. The coefficients are constant over a wide range of observed conditions: $\delta_{\rm air} = [-69,\ -72]$ ‰ and $\delta_{L0} = [9,\ 12]$ ‰.

4.4 Idealized experiments

Sensitivity experiments illustrate the effects of exchange with the environmental vapor, equilibrium fractionation, and kinetic diffusion on the isotopes. The same drop sizes as in Case CP are reused for all the experiments. In the first three experiments, the initial drop liquid and environmental vapor in the air are in isotopic equilibrium. The Control case has all three effects on the isotopes: exchange with the environmental vapor, equilibrium fractionation, and kinetic diffusion. The second case (OnlyDiff) has only environmental exchange and differential kinetic diffusion. Its equilibrium fractionation $\alpha_e = 1$ is artificially set to unity to suppress equilibrium fractionation. The third case (OnlyEq) has only environmental exchange and equilibrium fractionation. Its molecular diffusivity ratio K_m/K_{mi} is set to unity to suppress the diffusive kinetic effect. All the experiments have environmental exchange. Since these three cases have uniform subcloud air with $\delta = 0$, in equilibrium with the liquid drops ($\alpha_e^{-1} R_{air} = R_L = R_s$), environmental vapor exchange has the effect of simply relaxing back to $\delta = 0$.

Trajectories for drops with initial diameter $D_0 = 0.51$ mm, which evaporate completely just above the surface, are shown for these four experiments in Fig. 10. The black lines are the steady state end points for $n = 0$, 0.5, and 1, as in Fig. 5. The steady state end point depends on relative humidity over the drop h, which goes from 1 at cloud base to 0.89 at the surface.

The Control experiment (blue, Fig. 10), with all 3 effects, reaches the end point of $\delta_D > 5$‰ defined by $n = 1$. Differential isotope diffusion (OnlyDiff) and equilibrium fractionation (OnlyEq) mechanisms both enrich drops by similar amounts and the linear sum of these effects is only slightly less than their combined effect in the Control experiment. For kinetic diffusion without equilibrium fractionation (OnlyDiff: orange, Fig. 10), δ approaches a final value of +3 ‰. For equilibrium fractionation without diffusion (OnlyEq: green, Fig. 10), $\rho_i/\rho = 1$ is achieved by $K_m/K_{mi} = 1$, and isotopes increase by by +2 ‰, reaching the end point for $n = 0$ (black dot-dashed). Setting $n = 0$ also excludes differential diffusion. The end points increase downward due to decreasing relative humidity. About half of the effect of relative humidity on the end point is counteracted by reduction of $\alpha_e^{-1} = \alpha_{eL/V}$ with increasing temperature.

These experiments (Control, OnlyDiff, OnlyEq; Fig. 11) are repeated for the environmental air depleted by $\delta = -1$ ‰ relative to equilibrium over the initial drop. The exchange process immediately acts to deplete the drops toward $\delta = -1$. A fourth case (NoEqNoDiff, red Fig. 11) with only environmental exchange (having both equilibrium fractionation and differential diffusion disabled by setting to unity $\alpha_e = 1$ and $K_{mi}/Km = 1$) illustrates this, relaxing to $\delta_{v,air} = -1$ ‰ with a length scale of 40 m below cloud base, even for the relatively large drop ($D_0 = 0.51$ mm). If $\delta_{l0} = \delta_{v,air} = 0$ then the drop in NoEqNoDiff would trivially maintain $\delta = 0$ (not shown).

Experiments Control, OnlyDiff, and OnlyEq for this relatively depleted environment also are initially depleted by the exchange. After the initial depletion, the drops in the experiments enrich by equilibrium fractionation and/or differential diffusion processes, respectively, for each experiment. The depleted environmental vapor also shifts the end points by −1‰. As before, OnlyEq approaches the end point for $n = 0$, and Control approaches the end point for $n = 1$.

The depletion by exchange process opposite the enrichment by the equilibrium and diffusion processes results in non-monotonic adjustment that depends on the drop size

Figure 10. Deuterium isotope δ of drops of initial diameter $D_0 = 0.51$ mm and isotope ratio $\delta = 0$ for three experiments with air in isotopic equilibrium with the initial drop liquid isotope ratio $\delta_{L0} = \delta_{air} = 0$ ‰: Control (solid blue) includes exchange, equilibrium fractionation, and differential diffusion; OnlyDiff (orange) includes equilibrium and diffusion; and OnlyEq (green) includes exchange and diffusion. The dashed blue line shows the linear superposition δ sum of OnlyDiff and OnlyEq.

Figure 11. Deuterium isotope experiments Control (solid blue), OnlyDiff (orange), and OnlyEq (green) as in Fig. 10 but with environmental air depleted by -1 ‰ compared to equilibrium over the drop. A fourth experiment, NoEqNoDiff (red), has only exchange with air. Purple lines show results for different drop sizes, with smaller drops adjusting over shorter displacements.

(purple, Fig. 11). Smaller drops exchange faster, reach a minimum isotope ratio, then enrich faster by isotopic equilibrium fractionation and diffusion. Larger drops fall fast and adjust relatively slowly. Thus the isotope ratio trajectories cross for drops of different initial sizes.

The sensitivity studies demonstrate that the exchange and kinetic effects in the CG evaporation model make a significant difference to the results. The CG model is not significantly more complex than a Rayleigh model. Microphysics also makes a difference: Changing the DSD determines which drops evaporate completely having a profound effect on the resulting vapor.

5 Conclusion

When rain evaporates below cloud base, the *liquid* nearly reaches an equilibrium by exchange with vapor in the surrounding air. This equilibrium is not the thermodynamic "saturation" equilibrium of vapor enclosed over a liquid surface, but rather is analogous to the wet bulb temperature that drops also approach. The nearness of the drops to this equilibrium with their surroundings results in surface precipitation whose isotope ratio is mainly determined by the subcloud vapor. This exchange of the rain with rel-

atively enriched subcloud vapor explains the observed correlation of the precipitation isotope ratio to the local surface humidity (Crawford et al. 2017).

On the other hand, the hydrometeor source of *vapor* to the air is nearly the original liquid, because the bulk of the water mass evaporated is from large fractions of evaporation of individual drops. The temporary enrichment of vanishing drops, and its enhancement by diffusion, is an interesting flourish in the process that does not ultimately change the isotope ratio of the water that becomes vapor.

The Craig and Gordon (1969) equation models exchange with the environment, equilibrium evaporation, and turbulent and molecular diffusion. This combination of effects has a profound effect on the isotope fractionation, strongly enriching drops compared to equilibrium mixing or Rayleigh distillation.

We extend the work of Stewart (1975) by accounting for the drop size distribution and resolving the kinetic effects associated with diffusion in the drop-vapor laminar boundary layer. Assuming a spherical laminar layer around the drop, we parameterize the diameter-dependent ratio of molecular and turbulent vapor diffusion matched to previous experimental results. This diffusion model predicts relatively stronger molecular diffusion and kinetic enrichment for small drops. Drops become more enriched as they vanish, by 42% more than predicted by constant $n \approx 0.58$, previously measured for drops larger than 1 mm diameter. Laboratory and field observations are needed to test our parameterization over a wider range of drop diameters. Modeling the diffusion has several broader applications: it yields the humidity as a function of distance from an isolated drop, and it can be used to account for the effect of diffusive conduction and evaporation on drop temperature.

Small evaporating sea spray droplets (D =0.01-1.0 mm) would be enriched by these kinetic effects. Modeling the evaporation of sea spray must also include the effect of the concentrated salt solution, which is beyond the scope of this article, but measurement of the stable isotopes in surface atmospheric water vapor, the surface ocean, and the sea spray would help constrain the rate of evaporation from the sea spray relative to evaporation from the surface.

A broad range of drop sizes in the DSD further enriches the isotope ratio of the evaporated water. The precocious complete evaporation of small drops enriches δ_D of the resulting vapor by +10 ‰ compared to a single drop. Because small drops evaporate quickly and completely, cumulative vapor evaporated from realistic drop size distributions become enriched quickly to δ=-20 ‰ even with a large fraction $f \approx 0.95$ of the rain remaining.

The rain isotope flux divergence yields the isotope source representative of undiluted evaporative downdraft cores. Decomposition of the deuterium rain flux divergence demonstrates that evaporation and equilibration with the surrounding vapor enriches drops, and the evaporation of these drops enriches the subcloud air deuterium by 12 ‰ per 1 mm of rain accumulation. Secondarily, the rain transports relatively less enriched liquid downward.

The model formulated by following the Lagrangian trajectories of drops resolved by their initial size and stable isotope ratio is conceptually and computationally expedient for evaluating rain evaporation and its resulting vapor. The prediction of rain mass evaporation is more computationally expensive than the isotopes, but solutions are simple nearly elliptical curves. The model can be evaluated for over large steps, or at high resolution, enabling computation of sources of stable isotopes by the rain, which can be used interpret observations and models of rain, evaporated water vapor, and their stable water isotopes.

Appendix A The laminar length scale l_ν

In a laminar layer of thickness l_ν the rare water vapor isotopologue diffuses slower than the abundant vapor. Beyond this laminar layer, eddy diffusivity dominates, which diffuses both isotopologues equally. We parameterize the laminar layer thickness as

$$l_\nu = \nu/U$$

with kinematic viscosity ν and velocity scale U.

The velocity scale U is the speed of the drop relative to the surrounding air. U is usually found from the fall velocity of the drop. Small droplets (Reynolds number $Re = DU/\nu < 1$) fall with the weak velocity Stokes solution. Turbulent air velocities also accelerate the droplets, resulting in relative velocities.

We first neglect gravity and consider a velocity component of the droplet u suspended in air with velocity u_{air}. The relative speed in this component is $u' = u_{air} - u$. The inertia of the drop is balanced by the drag by the surrounding air:

$$m\frac{du}{dt} = \frac{\pi}{6}\hat{\rho}_l D^3 \frac{du}{dt} = \frac{\pi}{8}\hat{\rho} D^2 C_D (u_{air} - u)|u_{air} - u|$$

so

$$\frac{du}{dt} = \frac{3}{4}\frac{\hat{\rho}}{\hat{\rho}_l}\frac{C_D}{D}(u_{air} - u)|u_{air} - u|$$

Multiplying the equation of motion by the relative velocity u', we write the eddy kinetic energy $\overline{u'^2}/2$ equation. Neglecting correlations between anomalies u and u_{air},

$$\frac{d}{dt}\frac{\overline{u'^2}}{2} = -k|u'^3| = -k|\overline{u_{air}^3} - \overline{u^3}|$$

with

$$k = \frac{3}{4}\frac{\hat{\rho}}{\hat{\rho}_l}\frac{C_D}{D}.$$

Though the turbulence can drive temporary velocity anomalies, mean relative velocity kinetic energy strictly dissipates by drag. Its decay rate goes to zero when the third moments of air and drop velocity balance: $\overline{u_{air}^3} = \overline{u^3}$. Though the third moments are not equivalent to second moments, we assume the third moments are equal when the variances are equal $\overline{u_{air}^2} = \overline{u^2}$.

The turbulent kinetic energy TKE is proportional to any one component of the air velocity,

$$\overline{u_{air}^2} = 2\mathrm{TKE}/3.$$

The air and drop velocities are uncorrelated so

$$\overline{u'^2} = \overline{(u - u_{air})^2} = \overline{u^2} + \overline{u_{air}^2} = 2\overline{u_{air}^2} = 4\mathrm{TKE}/3.$$

All three components of the velocity are geometrically orthogonal, and the mean fall velocity U_{fall} is statistically orthogonal, so their magnitudes add in quadrature,

$$U = (4\mathrm{TKE} + U_{\mathrm{fall}}^2)^{1/2}. \tag{A1}$$

This drop-relative velocity is used for calculation of the laminar length scale. The contribution of the TKE is small, compared to the fall velocity.

Appendix B Temperature and humidity of the drop and environment

B1 Saturation deficit

Drops nearly approach the wet bulb temperature (Stewart, 1975) in an environment of uniform specific humidity q and adiabatic temperature. We first rewrite 1 by

noting the kinematic vapor diffusivity in air is $K_{va} = k_{va}/\hat{\rho}$ and $\Delta\hat{\rho}_v/\hat{\rho} = \Delta q = q_s(T_r) - q_a$ so

$$\frac{dD}{dz} = \frac{4 f_v k_{va}}{D U_{\rm fall} \hat{\rho}_l} \Delta q.$$

We linearize the local saturation specific humidity $q_s(T_r)$ of the drop about a representative temperature $\tilde{T}$. The humidity of the air $q_a = q_s(T_0)$ is saturated at the cloud base at temperature T_0. The linearization for Δq about $\tilde{T}$ is

$$\Delta q = q_s(T_r) - q_a = \left(\frac{\partial q_s}{\partial T}\right)_{\tilde{T}} (T_r - \tilde{T}) - q_a.$$

The drop temperature is very near the wet bulb temperature of the environment, yielding

$$\Delta q = \left(\frac{\partial q_s}{\partial T}\right)_{\tilde{T}} \Gamma_w (z' - \tau_w U_{\rm fall})$$

where $z' = z_0 - z > 0$ is the displacement fallen from cloud base, and

$$\Gamma_w = \Gamma_{\rm ad} \left(1 + L(\partial q_s/\partial T)_{\tilde{T}}/c_p\right)^{-1}$$

is the linearized lapse rate of wet bulb potential temperature. The adiabatic lapse rate is $\Gamma_{\rm ad} = g/c_p$. This approximates the linear profile of RH used by Sarkar et al. (2023). The heat transport length scale $\lambda = \tau_w U_{\rm fall}$ is the small downward displacement of cooler wet bulb temperature by the falling drop. It is largest (32 m) for the largest drops at cloud base (Appendix B), which is considerably smaller than turbulent displacements. The turbulence and the small heat transport displacement shall be neglected for convenience.

B2 Drop temperature

A falling drop evolves toward a wet bulb temperature. Its temperature equation is

$$\frac{dT}{dt} = -\frac{12 f_T K_{Ta} \hat{\rho} c_p}{D^2 \hat{\rho}_l c_w} \left[(T - T_a) + \frac{L}{c_p} \frac{f_v K_{va}}{f_h K_{Ta}} (q_s(T) - q_a)\right], \tag{B1}$$

with kinematic conductivity $K_{Ta} = k_{Ta}/(\hat{\rho} c_p)$, vapor diffusivity in air K_{va} [m^2 s^{-1}], density $\hat{\rho}_l$ and specific heat of liquid water c_w, drop diameter D, and specific humidity $q = \hat{\rho}_v/\hat{\rho}$. Solution and surface tension effects are important for very small droplets and concentrated solutions (e.g., haze and sea spray; Andreas, 1995), but these effects are neglected here. Radiative heating is also neglected. For typical temperature and pressure below the cloud, $K_{va}/K_{Ta} = 1.16$.

The conventional wet bulb temperature T_{w0} is defined by $c_p(T_{w0} - T_a) = -L(q_s(T_{w0}) - q_a)$ but inspection of equation B1 shows that the equilibrium wet bulb temperature of a drop is slightly modified by the ratios, of vapor to temperature, of ventilation factors and diffusivities,

$$T_w = T_a - (L/c_p)(f_v K_{va}/f_h K_{Ta})(q_s(T_w) - q_a). \tag{B2}$$

It still depends mostly on the environment T_a, q_a, and slightly on the diameter through the ventilation factors. The ratio of the ventilation factors f_v/f_h is nearly unity (Abraham, 1962). This effect is parameterized in the body of the paper by $n = \rho_m/rho$. The diffusivity ratio $K_{va}/K_{Ta} = 1.16$ results in a 6% increase of the air-drop temperature difference $T_a - T_w$ compared to $T_a - T_{w0}$.

The wet bulb temperature is practical to measure, yet it cannot be found analytically from air temperature and humidity because the empirical equilibrium humidity ($q_s(T)$) cannot be inverted analytically. Corpart et al. (2023) solve for the drop temperature by approximating the equilibrium humidity by a quadratic. Calculating the derivative $\partial q_s/\partial T$) by automatic differentiation, we solve equation B2 numerically within 10^{-3} K in two iterations of Newton's method.

How fast does the drop approach T_w? The time scale for temperature conduction is

$$\tau_T = \left(\frac{12 f_h K_{Ta} \hat{\rho} c_p}{D^2 \hat{\rho}_l c_w} \right)^{-1}.$$

The wet bulb adjustment is faster because of the evaporative heating term. Linearizing the saturation specific humidity about the wet bulb temperature, T_w, $q - q_s(T_w) = (\partial q_s / \partial T)_{T_w}(T - T_w)$, we find the temperature equation adjusts as,

$$\frac{dT}{dt} = -(T - T_w)(1 + \beta)/\tau_T = -(T - T_w)/\tau_w$$

with

$$\beta = \frac{L}{c_p} \frac{f_v K_{va}}{f_T K_{Ta}} \left(\frac{\partial q_s}{\partial T} \right)_{T_w} \approx \frac{L}{c_p} \left(\frac{\partial q_s}{\partial T} \right)_{T_w}.$$

The conductive-evaporative temperature adjustment timescale for the drop is

$$\tau_w = \tau_T / (1 + \beta), \tag{B3}$$

which is $(1+\beta) \sim 2.8$ times shorter than τ_T at $T = 290$ K. This timescale will be used to compute the distance drops fall as their temperature adjusts.

Fall transport

Drops are cooler than the local wet bulb temperature of their environment, because they fall from the cooler environment aloft. In the drop's frame of reference, T_w of the environment warms as the drop descends

$$\left(\frac{dT_w}{dt} \right)_{\text{fall}} = +U_{\text{fall}} \Gamma_w$$

with lapse rate $\Gamma_w = dT_w/dz < 0$ and downward velocity $U_{\text{fall}} = -dz/dt > 0$. The equilibrium depression from the wet bulb temperature $\Delta T = T - T_w$ is solved by balancing this falling source and the evaporative-conductive temperature source above:

$$0 = \frac{d}{dt}\Delta T = \left(\frac{d}{dt}\Delta T \right)_{\text{evap-cdct}} + \left(\frac{d}{dt}\Delta T \right)_{\text{fall}} = -\Delta T/\tau_w + U_{\text{fall}} \Gamma_w.$$

The drop temperature T is cooler than the surrounding wet bulb temperature T_w because the drop T adjusts to the environmental T_w over an integral length scale $\lambda = \tau_w U_{\text{fall}}$, and

$$T = T_w + \lambda \Gamma_w.$$

The adjustment length scale λ is largest for large drops, reaching 30 m for drops $D >$ 1 mm. This diagnoses a 1.0 mm drop has temperature $T = T_w - 0.2$ K and 0.1 mm drop has $T = T_w - 0.001$ K. The difference $T - T_w$ is also small in numerical integrations of B1. The adjustment length scale has been neglected in calculations in the body of this paper.

Open Research

The NOAA PSL surface meteorology data (NOAA Physical Sciences Laboratory, 2020), the water isotope analyzer data (Bailey and Noone, 2021), and the rainwater isotope analysis data (Quiñones Meléndez et al., 2022) from the *Ronald H. Brown* and EUREC4A-ATOMIC field experiment are accessible from their respective references. Computational notebooks written in the Julia language (Bezanson et al., 2017) are publicly archived (de Szoeke, 2024).

Acknowledgments

This work was supported by NSF award number 1937780 and NOAA award number NA19OAR4310375 (SPD, DN), and ONR award number N000142212042 (SPD). This material is based upon work supported by the National Science Foundation under Grant No. AGS-1938108 (PNB).

References

Abraham, F. F. (1962). Evaporation of raindrops. *Journal of Geophysical Research (1896-1977)*, *67*(12), 4673–4682. Retrieved 2024-01-23, from https://onlinelibrary.wiley.com/doi/abs/10.1029/JZ067i012p04673 (_eprint: https://onlinelibrary.wiley.com/doi/pdf/10.1029/JZ067i012p04673) doi: 10.1029/JZ067i012p04673

Abraham, F. F., Jordan, S. K., Kortzeborn, R. N., & Kolsky, H. G. (1972, March). Model for Time-dependent Raindrop Size Distributions; Application to the Washout of Airborne Contaminants. *IBM Journal of Research and Development*, *16*(2), 91–100. Retrieved 2024-01-23, from https://ieeexplore.ieee.org/document/5391467?denied= (Conference Name: IBM Journal of Research and Development) doi: 10.1147/rd.162.0091

Andreas, E. L. (1995, April). The Temperature of Evaporating Sea Spray Droplets. *Journal of the Atmospheric Sciences*, *52*(7), 852–862. Retrieved 2023-10-30, from https://journals.ametsoc.org/view/journals/atsc/52/7/1520-0469_1995_052_0852_ttoess_2_0_co_2.xml (Publisher: American Meteorological Society Section: Journal of the Atmospheric Sciences) doi: 10.1175/1520-0469(1995)052⟨0852:TTOESS⟩2.0.CO;2

Bailey, A., Aemisegger, F., Villiger, L., Los, S. A., Reverdin, G., Quiñones Meléndez, E., ... Thompson, E. J. (2023, January). Isotopic measurements in water vapor, precipitation, and seawater during EUREC^{4}A. *Earth System Science Data*, *15*(1), 465–495. Retrieved 2024-02-07, from https://essd.copernicus.org/articles/15/465/2023/ (Publisher: Copernicus GmbH) doi: 10.5194/essd-15-465-2023

Bailey, A., & Noone, D. (2021). *ATOMIC ship water vapor isotopic analyzer: Near-surface humidity and water vapor isotope ratios from an isotopic analyzer aboard NOAA Ship Ronald H. Brown in the North Atlantic Ocean, near Barbados: Atlantic Tradewind Ocean-Atmosphere Mesoscale Interaction Campaign 2010-01-26 to 2020-02-10 (NCEI Accession 0225417).* NOAA National Centers for Environmental Information. Retrieved 2024-02-20, from https://doi.org/10.25921/s76r-1n85. (ItemType: dataset) doi: 10.25921/s76r-1n85

Best, A. C. (1952). The evaporation of raindrops. *Quarterly Journal of the Royal Meteorological Society*, *78*(336), 200–225. Retrieved 2024-01-22, from https://onlinelibrary.wiley.com/doi/abs/10.1002/qj.49707833608 (_eprint: https://onlinelibrary.wiley.com/doi/pdf/10.1002/qj.49707833608) doi: 10.1002/qj.49707833608

Bezanson, J., Edelman, A., Karpinski, S., & Shah, V. B. (2017, January). Julia: A Fresh Approach to Numerical Computing. *SIAM Review*, *59*(1), 65–98. Retrieved 2024-02-20, from https://epubs.siam.org/doi/10.1137/141000671 (Publisher: Society for Industrial and Applied Mathematics) doi: 10.1137/141000671

Brutsaert, W. (1965). A model for evaporation as a molecular diffusion process into a turbulent atmosphere. *Journal of Geophysical Research (1896-1977)*, *70*(20), 5017–5024. Retrieved 2024-02-20, from https://onlinelibrary.wiley.com/doi/abs/10.1029/JZ070i020p05017 (_eprint: https://onlinelibrary.wiley.com/doi/pdf/10.1029/JZ070i020p05017) doi: 10.1029/JZ070i020p05017

Brutsaert, W. (1975, October). The Roughness Length for Water Vapor Sensible Heat, and Other Scalars. *Journal of the Atmospheric Sciences*, *32*(10), 2028–2031. Retrieved 2020-08-21, from https://journals.ametsoc.org/jas/article/32/10/2028/18389/The-Roughness-Length-for-Water-Vapor-Sensible-Heat (Publisher: American Meteorological Society) doi: 10.1175/1520-0469(1975)032⟨2029:TRLFWV⟩2.0.CO;2

Corpart, M., Restagno, F., & Boulogne, F. (2023, October). Analytical prediction

of the temperature and the lifetime of an evaporating spherical droplet. *Colloids and Surfaces A: Physicochemical and Engineering Aspects*, *675*, 132059. Retrieved 2024-01-22, from https://www.sciencedirect.com/science/article/pii/S0927775723011433 doi: 10.1016/j.colsurfa.2023.132059

Craig, H., & Gordon, L. I. (1965). Deuterium and oxygen 18 variations in the ocean and the marine atmosphere. In Tongiorgi, E. (Ed.), *Stable Isotopes in Oceanographic Studies and Palaeotemperatures* (pp. 9–130). Pisa: Lab. Geologia Nucleare.

Crawford, J., Hollins, S. E., Meredith, K. T., & Hughes, C. E. (2017). Precipitation stable isotope variability and subcloud evaporation processes in a semi-arid region. *Hydrological Processes*, *31*(1), 20–34. Retrieved 2024-02-25, from https://onlinelibrary.wiley.com/doi/abs/10.1002/hyp.10885 (_eprint: https://onlinelibrary.wiley.com/doi/pdf/10.1002/hyp.10885) doi: 10.1002/hyp.10885

Dansgaard, W. (1964, November). Stable isotopes in precipitation. *Tellus*, *16*(4), 436–468. Retrieved 2022-04-08, from http://tellusa.net/index.php/tellusa/article/view/8993 doi: 10.1111/j.2153-3490.1964.tb00181.x

de Szoeke, S. P. (2024). *Shallow cumulus rain drop evaporation and isotope model notebooks* [Software: Julia Jupyter computational notebooks]. Retrieved from https://ir.library.oregonstate.edu/concern/datasets/br86bc57n (Publisher: Oregon State University) doi: 10.7267/br86bc57n

Galewsky, J., Steen-Larsen, H. C., Field, R. D., Worden, J., Risi, C., & Schneider, M. (2016). Stable isotopes in atmospheric water vapor and applications to the hydrologic cycle. *Reviews of Geophysics*, *54*(4), 809–865. Retrieved 2022-04-08, from https://onlinelibrary.wiley.com/doi/abs/10.1002/2015RG000512 (_eprint: https://onlinelibrary.wiley.com/doi/pdf/10.1002/2015RG000512) doi: 10.1002/2015RG000512

Garratt, J. R. (1992). *The atmospheric boundary layer*. Cambridge.

Gat, J. R. (1996). Oxygen and Hydrogen Isotopes in the Hydrologic Cycle. *Annual Review of Earth and Planetary Sciences*, *24*(1), 225–262. Retrieved 2022-12-06, from https://doi.org/10.1146/annurev.earth.24.1.225 (_eprint: https://doi.org/10.1146/annurev.earth.24.1.225) doi: 10.1146/annurev.earth.24.1.225

Graf, P., Wernli, H., Pfahl, S., & Sodemann, H. (2019, January). A new interpretative framework for below-cloud effects on stable water isotopes in vapour and rain. *Atmospheric Chemistry and Physics*, *19*(2), 747–765. Retrieved 2023-12-06, from https://acp.copernicus.org/articles/19/747/2019/ (Publisher: Copernicus GmbH) doi: 10.5194/acp-19-747-2019

Hiron, T., & Flossmann, A. I. (2020). Oxygen Isotopic Fractionation in Clouds: A Bin-Resolved Microphysics Model Approach. *Journal of Geophysical Research: Atmospheres*, *125*(21), e2019JD031753. Retrieved 2024-02-25, from https://onlinelibrary.wiley.com/doi/abs/10.1029/2019JD031753 (_eprint: https://onlinelibrary.wiley.com/doi/pdf/10.1029/2019JD031753) doi: 10.1029/2019JD031753

Kinzer, G. D., & Gunn, R. (1951). The evaporation, temperature and thermal relaxation-time of freely falling waterdrops. *Journal of Meteorology*, *8*(2), 71–83.

Lee, J.-E., & Fung, I. (2008). "Amount effect" of water isotopes and quantitative analysis of post-condensation processes. *Hydrological Processes*, *22*(1), 1–8. Retrieved 2024-01-24, from https://onlinelibrary.wiley.com/doi/abs/10.1002/hyp.6637 (_eprint: https://onlinelibrary.wiley.com/doi/pdf/10.1002/hyp.6637) doi: 10.1002/hyp.6637

Li, X., & Srivastava, R. C. (2001, September). An Analytical Solution for Raindrop Evaporation and Its Application to Radar Rainfall Measurements. *Journal*

of Applied Meteorology and Climatology, *40*(9), 1607–1616. Retrieved 2024-01-22, from https://journals.ametsoc.org/view/journals/apme/40/9/1520-0450_2001_040_1607_aasfre_2.0.co_2.xml (Publisher: American Meteorological Society Section: Journal of Applied Meteorology and Climatology) doi: 10.1175/1520-0450(2001)040⟨1607:AASFRE⟩2.0.CO;2

Merlivat, L. (1978). Molecular diffusivities of $H_2{}^{16}O$, $HD^{16}O$, and $H_2{}^{18}O$ in gases. *The Journal of Chemical Physics*, *69*(6), 2864–2871. Retrieved 2021-02-23, from https://aip.scitation.org/doi/abs/10.1063/1.436884 (Publisher: American Institute of Physics) doi: 10.1063/1.436884

Merlivat, L., & Jouzel, J. (1979, January). Global climatic interpretation of the deuterium-oxygen 18 relationship for precipitation. *Journal of Geophysical Research*, *84*, 5029–5033. doi: 10.1029/JC084iC08p05029

NOAA Physical Sciences Laboratory. (2020). *The Atlantic Tradewind Ocean-Atmosphere Mesoscale Interaction Campaign (ATOMIC), Barbados, Jan 17 - Feb 12, 2020. Ronald H. Brown Meteorology and Navigation.* NOAA National Centers for Environmental Information. Retrieved from https://www.ncei.noaa.gov/archive/accession/ATOMIC-2020

Noone, D. (2012). Pairing Measurements of the Water Vapor Isotope Ratio with Humidity to Deduce Atmospheric Moistening and Dehydration in the Tropical Midtroposphere. *Journal of Climate*, *25*(13), 4476–4494. Retrieved from http://journals.ametsoc.org/doi/abs/10.1175/JCLI-D-11-00582.1 doi: 10.1175/JCLI-D-11-00582.1

Noone, D., & Simmonds, I. (2002). Associations between δ18O of Water and Climate Parameters in a Simulation of Atmospheric Circulation for 1979–95. *Journal of Climate*, *15*(22), 3150–3169. Retrieved 2024-02-29, from https://journals.ametsoc.org/view/journals/clim/15/22/1520-0442_2002_015_3150_aboowa_2.0.co_2.xml (Publisher: American Meteorological Society Section: Journal of Climate) doi: 10.1175/1520-0442(2002)015⟨3150:ABOOWA⟩2.0.CO;2

Quinn, P. K., Thompson, E. J., Coffman, D. J., Baidar, S., Bariteau, L., Bates, T. S., ... Zuidema, P. (2021, April). Measurements from the RV *Ronald H. Brown* and related platforms as part of the Atlantic Tradewind Ocean-Atmosphere Mesoscale Interaction Campaign (ATOMIC). *Earth System Science Data*, *13*(4), 1759–1790. Retrieved 2023-10-19, from https://essd.copernicus.org/articles/13/1759/2021/ (Publisher: Copernicus GmbH) doi: 10.5194/essd-13-1759-2021

Quiñones Meléndez, E., de Szoeke, S. P., & David, N. (2022). *ATOMIC ship rain sampler : Rainwater isotope ratios from samples taken aboard NOAA Ship Ronald H. Brown in the North Atlantic Ocean, near Barbados: Atlantic Tradewind Ocean-Atmosphere Mesoscale Interaction Campaign 2020-01-05 to 2020-02-11 (NCEI Accession 0244402).* NOAA National Centers for Environmental Information. Retrieved 2024-02-20, from https://www.ncei.noaa.gov/access/metadata/landing-page/bin/iso?id=gov.noaa.nodc:0244402 (Last Modified: 2024-02-17) doi: 10.25921/bbje-6y41

Risi, C., Muller, C., & Blossey, P. (2021). Rain Evaporation, Snow Melt, and Entrainment at the Heart of Water Vapor Isotopic Variations in the Tropical Troposphere, According to Large-Eddy Simulations and a Two-Column Model. *Journal of Advances in Modeling Earth Systems*, *13*(4), e2020MS002381. Retrieved 2024-02-20, from https://onlinelibrary.wiley.com/doi/abs/10.1029/2020MS002381 (_eprint: https://onlinelibrary.wiley.com/doi/pdf/10.1029/2020MS002381) doi: 10.1029/2020MS002381

Salamalikis, V., Argiriou, A. A., & Dotsika, E. (2016, February). Isotopic modeling of the sub-cloud evaporation effect in precipitation. *Science of The Total Environment*, *544*, 1059–1072. Retrieved 2023-06-15, from https://

www.sciencedirect.com/science/article/pii/S0048969715310536 doi: 10.1016/j.scitotenv.2015.11.072

Sarkar, M., Bailey, A., Blossey, P., de Szoeke, S. P., Noone, D., Quiñones Meléndez, E., ... Chuang, P. Y. (2023, October). Sub-cloud rain evaporation in the North Atlantic winter trade winds derived by pairing isotopic data with a bin-resolved microphysical model. *Atmospheric Chemistry and Physics*, *23*(19), 12671–12690. Retrieved 2023-12-05, from https://acp.copernicus.org/articles/23/12671/2023/ (Publisher: Copernicus GmbH) doi: 10.5194/acp-23-12671-2023

Sengupta, S., Bhattacharya, S. K., Sunil, N. S., & Sonar, S. (2023, July). Quantifying Raindrop Evaporation Deficit in General Circulation Models from Observed and Model Rain Isotope Ratios on the West Coast of India. *Atmosphere*, *14*(7), 1147. Retrieved 2024-02-20, from https://www.mdpi.com/2073-4433/14/7/1147 (Number: 7 Publisher: Multidisciplinary Digital Publishing Institute) doi: 10.3390/atmos14071147

Stevens, B., Bony, S., Farrell, D., Ament, F., Blyth, A., Fairall, C., ... Zöger, M. (2021, August). EUREC^{4}A. *Earth System Science Data*, *13*(8), 4067–4119. Retrieved 2023-11-16, from https://essd.copernicus.org/articles/13/4067/2021/ (Publisher: Copernicus GmbH) doi: 10.5194/essd-13-4067-2021

Stewart, M. K. (1975). Stable isotope fractionation due to evaporation and isotopic exchange of falling waterdrops: Applications to atmospheric processes and evaporation of lakes. *Journal of Geophysical Research (1896-1977)*, *80*(9), 1133–1146. Retrieved 2023-02-03, from https://onlinelibrary.wiley.com/doi/abs/10.1029/JC080i009p01133 (_eprint: https://onlinelibrary.wiley.com/doi/pdf/10.1029/JC080i009p01133) doi: 10.1029/JC080i009p01133

Thurnherr, I., Kozachek, A., Graf, P., Weng, Y., Bolshiyanov, D., Landwehr, S., ... Aemisegger, F. (2020, May). Meridional and vertical variations of the water vapour isotopic composition in the marine boundary layer over the Atlantic and Southern Ocean. *Atmospheric Chemistry and Physics*, *20*(9), 5811–5835. Retrieved 2024-02-25, from https://acp.copernicus.org/articles/20/5811/2020/ (Publisher: Copernicus GmbH) doi: 10.5194/acp-20-5811-2020

Tremoy, G., Vimeux, F., Soumana, S., Souley, I., Risi, C., Favreau, G., & Oï, M. (2014). Clustering mesoscale convective systems with laser-based water vapor δ18O monitoring in Niamey (Niger). *Journal of Geophysical Research: Atmospheres*, *119*(9), 5079–5103. Retrieved 2024-02-25, from https://onlinelibrary.wiley.com/doi/abs/10.1002/2013JD020968 (_eprint: https://onlinelibrary.wiley.com/doi/pdf/10.1002/2013JD020968) doi: 10.1002/2013JD020968

Figure 1.

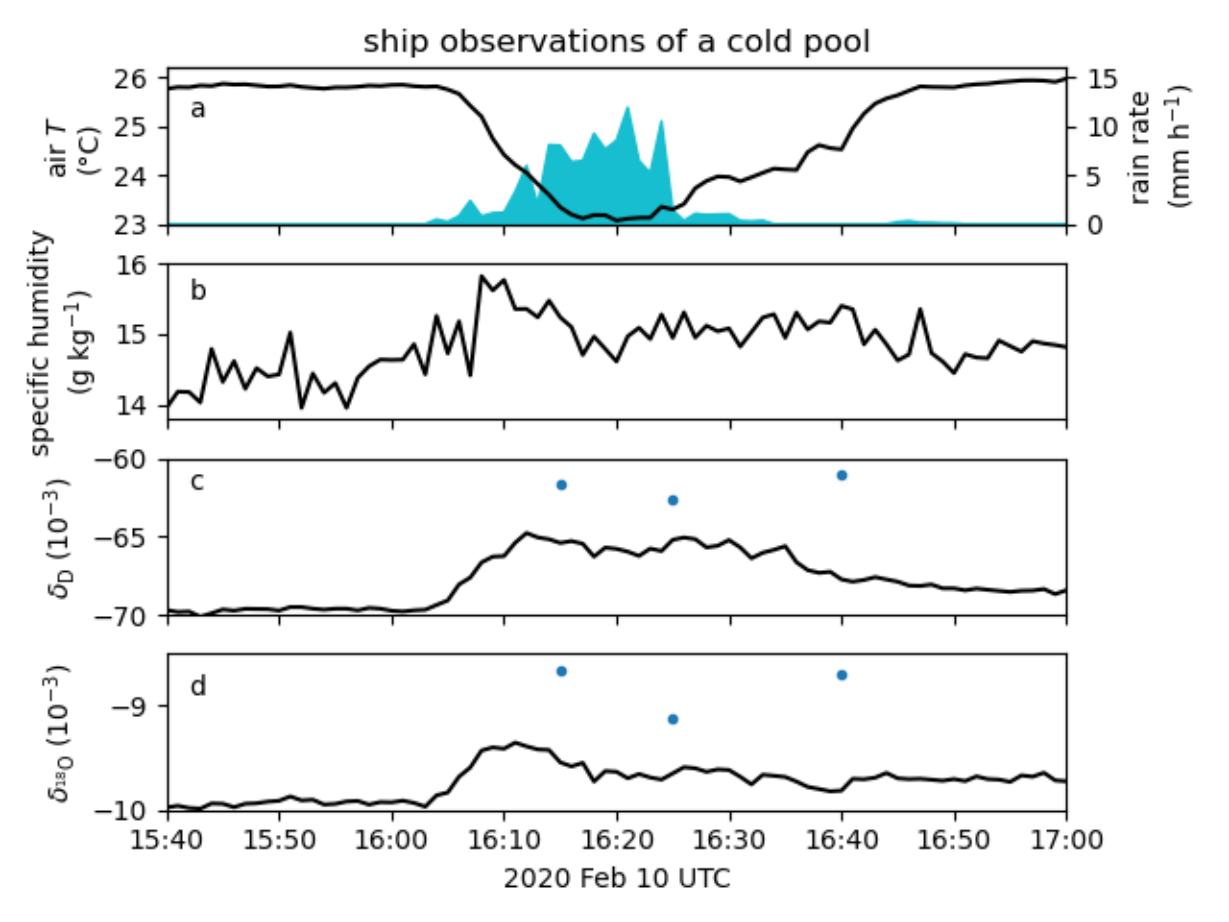
ship observations of a cold pool
a
air T (°C)
rain rate (mm h^{-1})
b
specific humidity (g kg^{-1})
c
δ_D (10^{-3})
d
δ_{18O} (10^{-3})
15:40
15:50
16:00
16:10
16:20
16:30
16:40
16:50
17:00
2020 Feb 10 UTC

Figure 2.

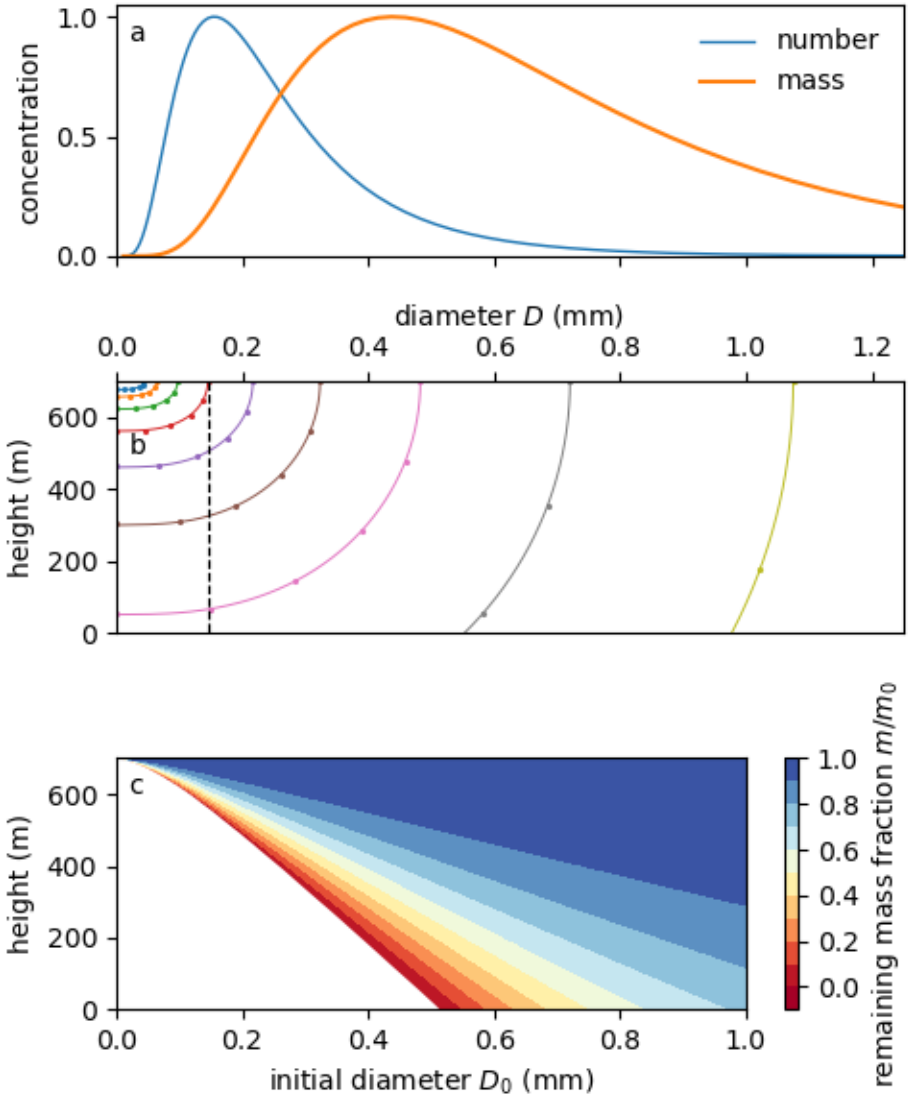
a
number
mass
concentration
1.0
0.5
0.0
diameter D (mm)
0.0
0.2
0.4
0.6
0.8
1.0
1.2
b
height (m)
600
400
200
0
c
height (m)
600
400
200
0
0.0
0.2
0.4
0.6
0.8
1.0
initial diameter D_0 (mm)
remaining mass fraction m/m_0
1.0
0.8
0.6
0.4
0.2
0.0

Figure 3.

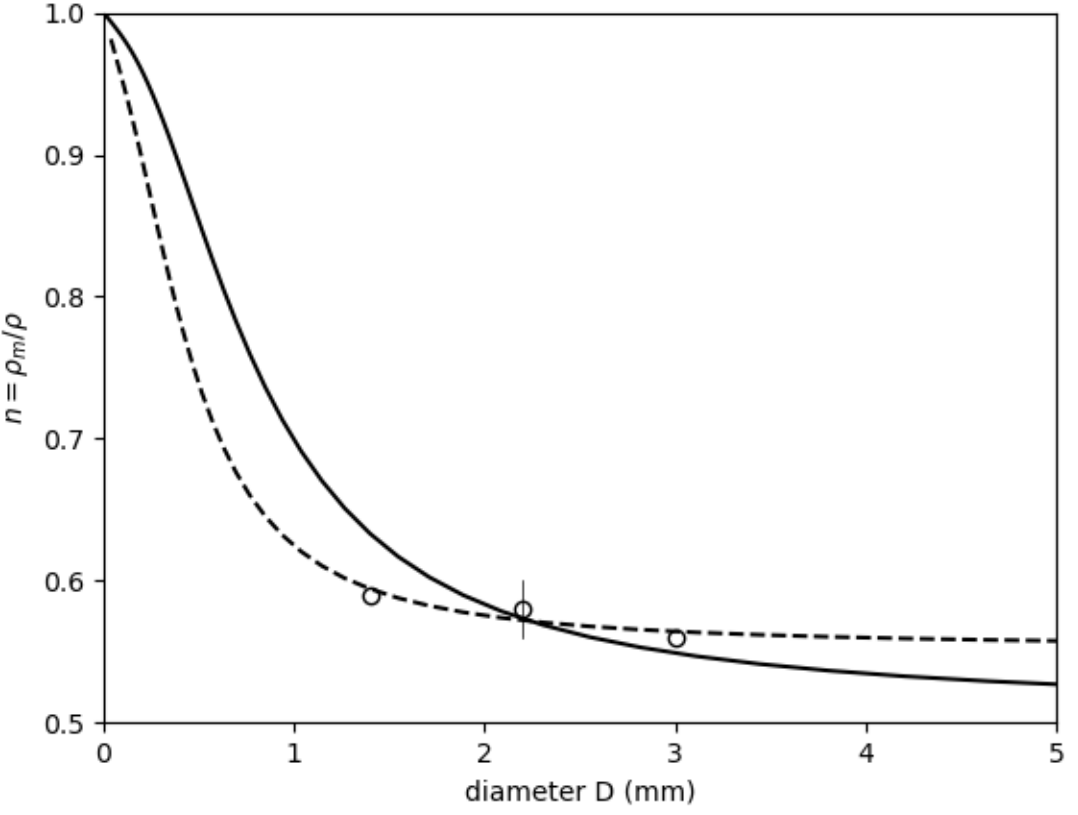
1.0
0.9
0.8
0.7
0.6
0.5
$n = \rho_m/\rho$
0
1
2
3
4
5
diameter D (mm)

Figure 4.

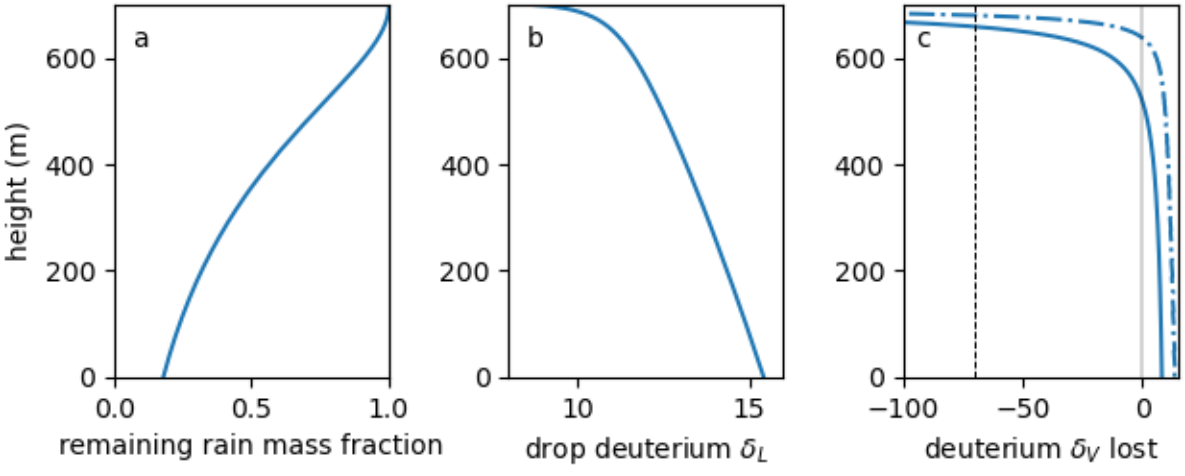
a
b
c
height (m)
0
200
400
600
0.0
0.5
1.0
remaining rain mass fraction
10
15
drop deuterium δ_L
−100
−50
0
deuterium δ_V lost

Figure 5.

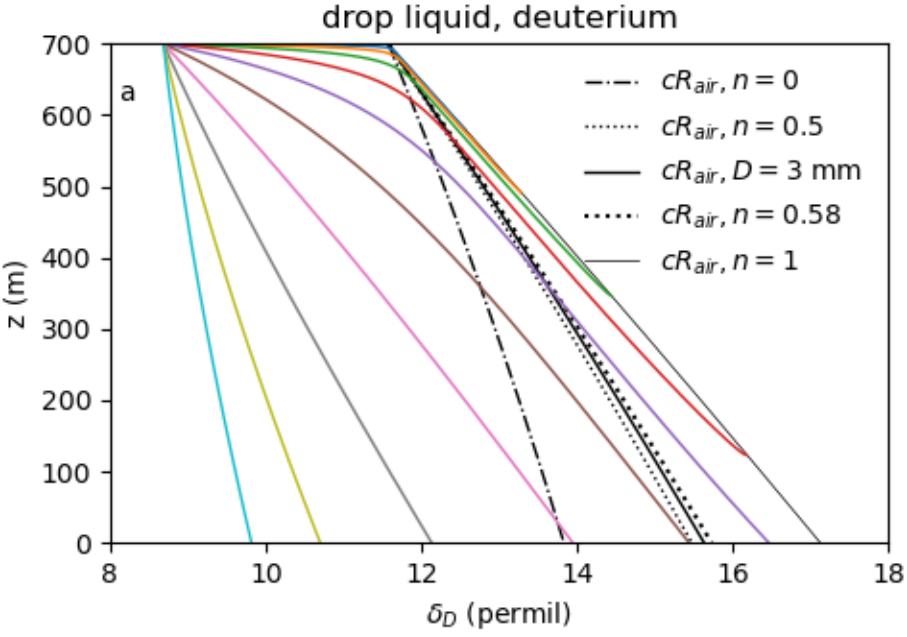
drop liquid, deuterium
a
$cR_{air}, n = 0$
$cR_{air}, n = 0.5$
$cR_{air}, D = 3$ mm
$cR_{air}, n = 0.58$
$cR_{air}, n = 1$
z (m)
δ_D (permil)

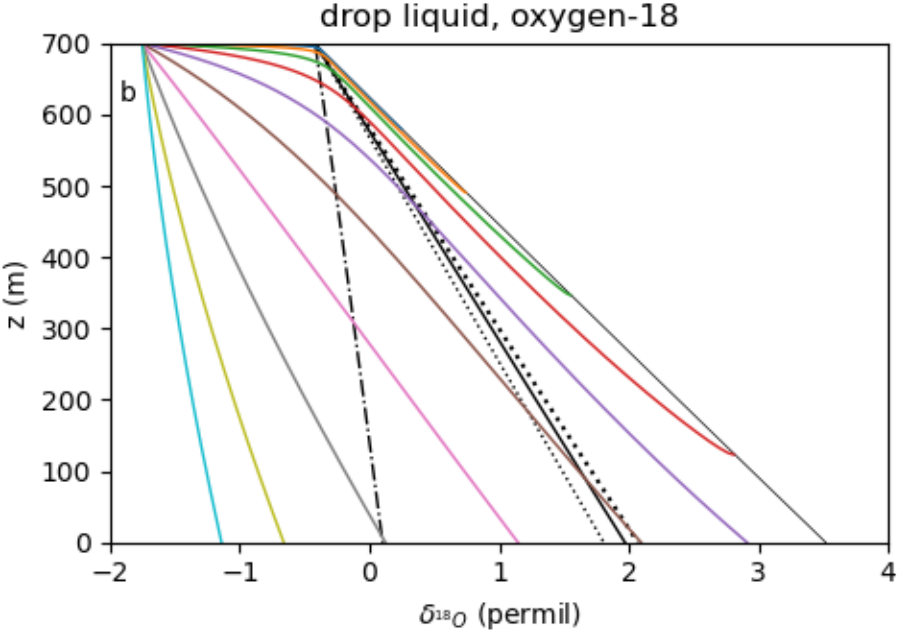
drop liquid, oxygen-18
b
z (m)
δ_{18O} (permil)

Figure 6.

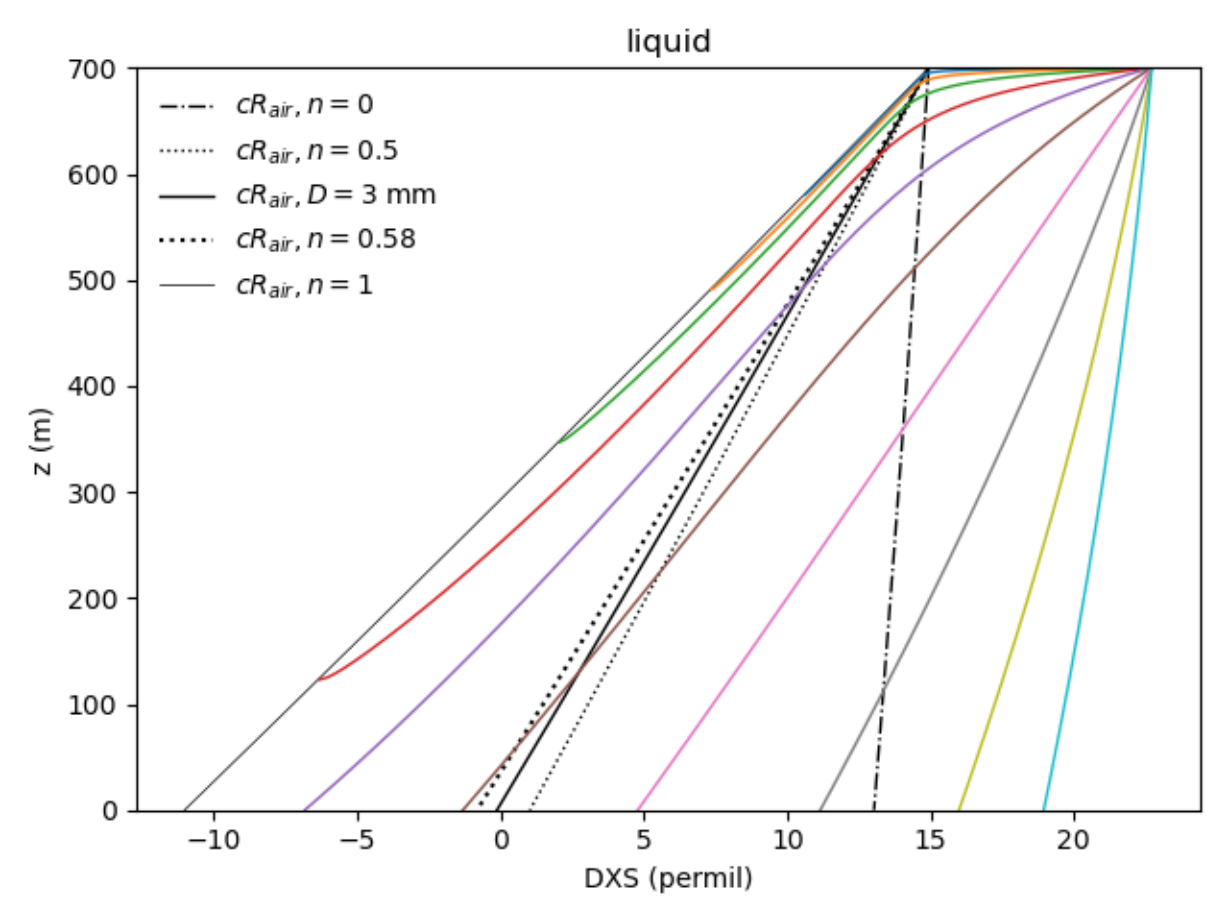
liquid
$cR_{air}, n = 0$
$cR_{air}, n = 0.5$
$cR_{air}, D = 3$ mm
$cR_{air}, n = 0.58$
$cR_{air}, n = 1$
z (m)
DXS (permil)
700
600
500
400
300
200
100
0
−10
−5
0
5
10
15
20

Figure 7.

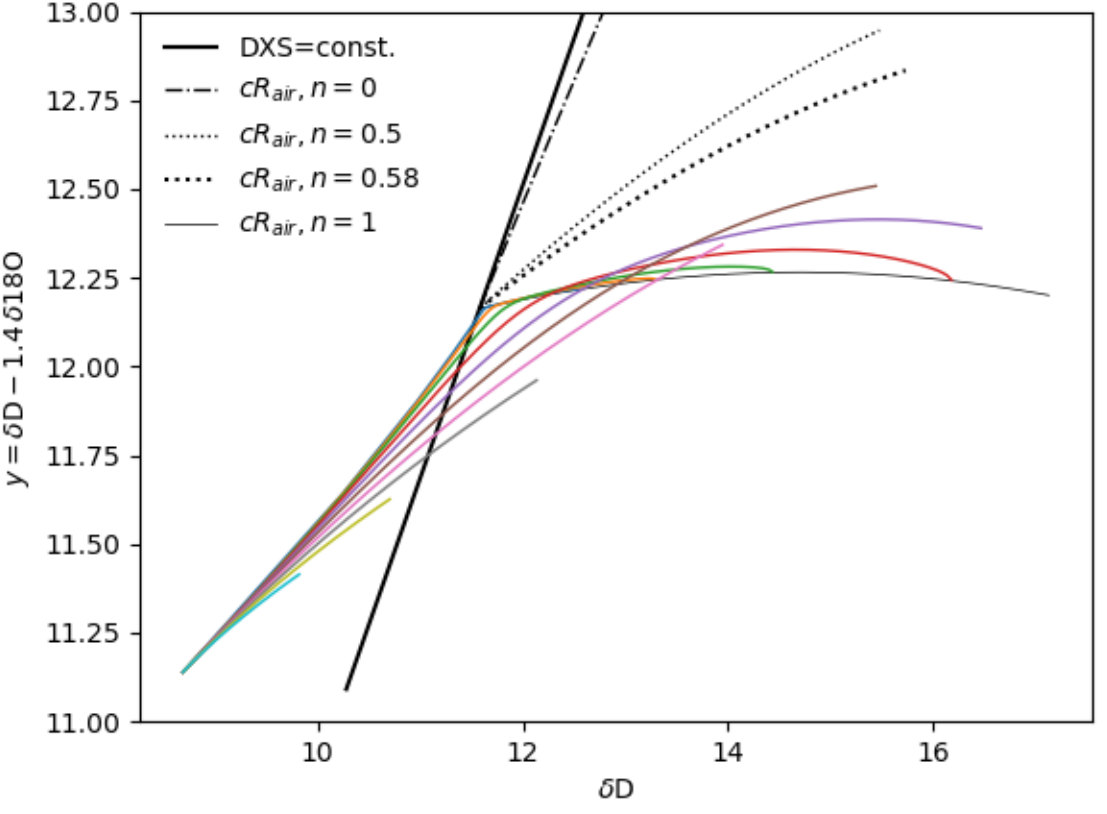
DXS=const.
$cR_{air}, n = 0$
$cR_{air}, n = 0.5$
$cR_{air}, n = 0.58$
$cR_{air}, n = 1$
$y = \delta D - 1.4\delta 18O$
δD
13.00
12.75
12.50
12.25
12.00
11.75
11.50
11.25
11.00
10
12
14
16

Figure 8.

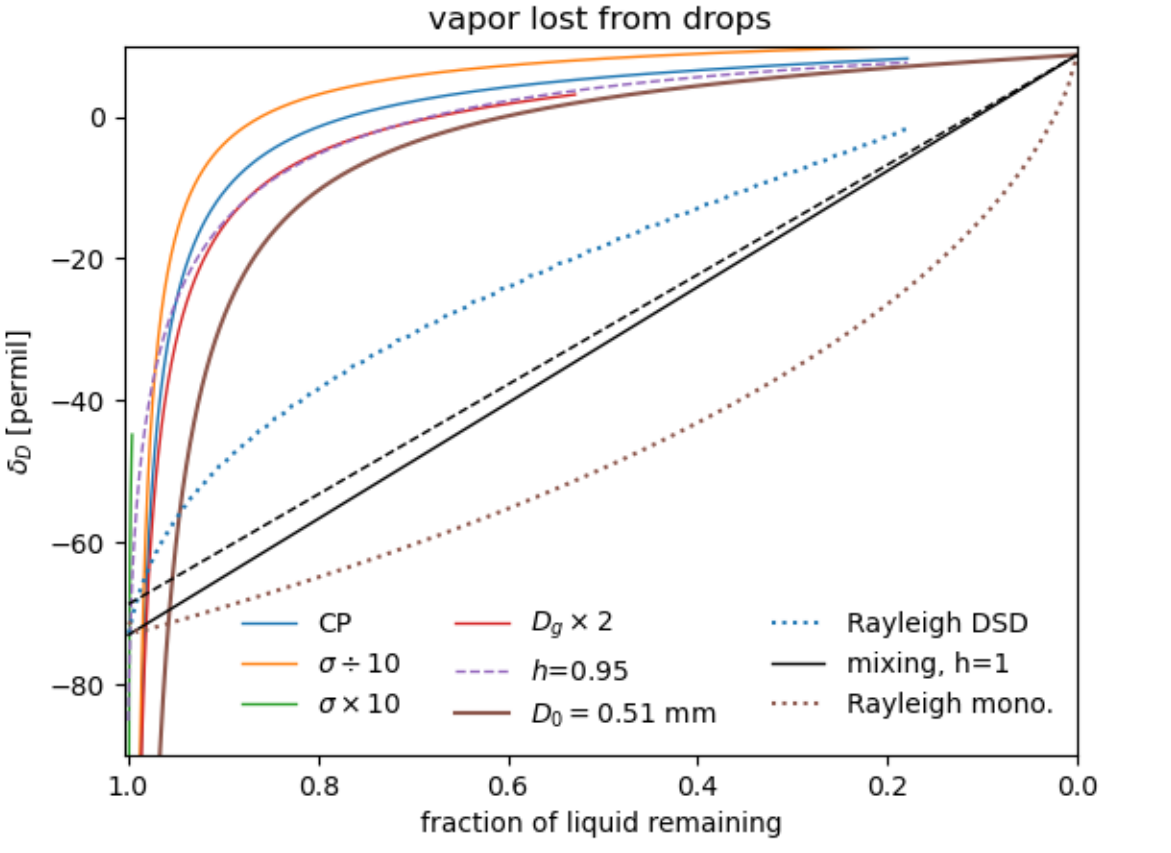
vapor lost from drops
0
−20
−40
−60
−80
δ_D [permil]
1.0
0.8
0.6
0.4
0.2
0.0
fraction of liquid remaining
CP
$\sigma \div 10$
$\sigma \times 10$
$D_g \times 2$
h=0.95
$D_0 = 0.51$ mm
Rayleigh DSD
mixing, h=1
Rayleigh mono.

Figure 9.

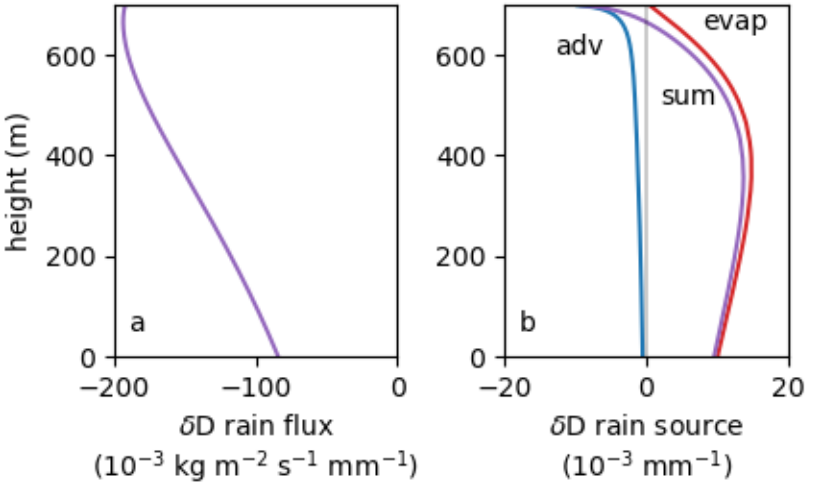
height (m)
600
400
200
0
a
−200
−100
0
δD rain flux
(10^{-3} kg m^{-2} s^{-1} mm^{-1})
b
adv
evap
sum
−20
0
20
δD rain source
(10^{-3} mm^{-1})

Figure 10.

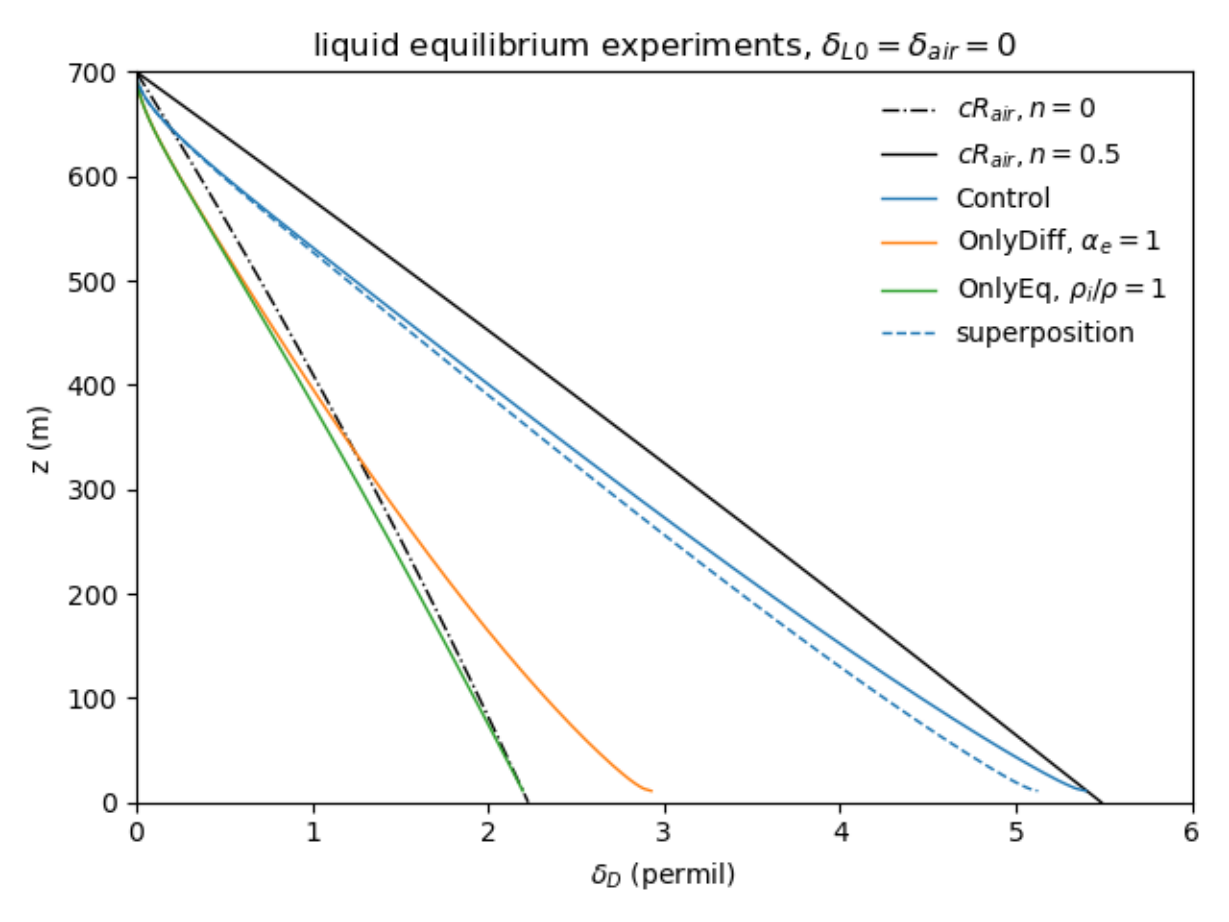
liquid equilibrium experiments, $\delta_{L0} = \delta_{air} = 0$
$cR_{air}, n = 0$
$cR_{air}, n = 0.5$
Control
OnlyDiff, $\alpha_e = 1$
OnlyEq, $\rho_l/\rho = 1$
superposition
z (m)
δ_D (permil)
0
100
200
300
400
500
600
700
0
1
2
3
4
5
6

Figure 11.

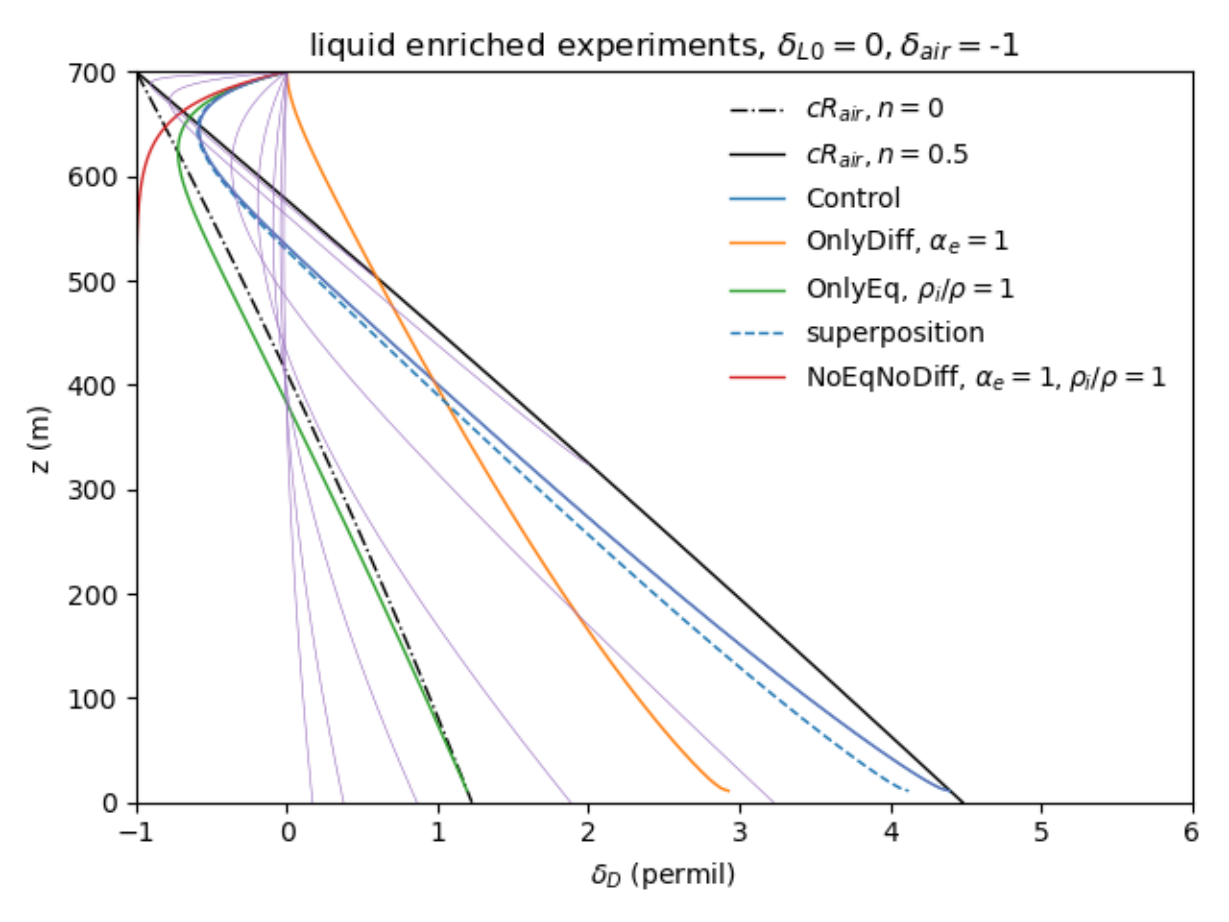
liquid enriched experiments, $\delta_{L0} = 0$, $\delta_{air} = -1$
cR_{air}, $n = 0$
cR_{air}, $n = 0.5$
Control
OnlyDiff, $\alpha_e = 1$
OnlyEq, $\rho_i/\rho = 1$
superposition
NoEqNoDiff, $\alpha_e = 1$, $\rho_i/\rho = 1$
z (m)
δ_D (permil)
700
600
500
400
300
200
100
0
−1
0
1
2
3
4
5
6